construction materials

MDPI

Article

Shear Performance of Reinforced Concrete Beams with Varying Recycled Coarse and Fine Aggregate Contents Under Fire Exposure

Mu'tasim Abdel-Jaber [1,*], Mousa Shhabat [1,2], Ahmed Ashteyat [3,1], Ahmad Al-Khreisat [4] and Omar Shehabat [5]

[1] Department of Civil Engineering, Faculty of Engineering, The University of Jordan, Amman 11942, Jordan; mos8200833@ju.edu.jo (M.S.); a.ashteyat@ju.edu.jo (A.A.)
[2] Greater Irbid Municipality, Irbid 21110, Jordan
[3] Department of Civil Engineering, College of Engineering in Al-Kharj, Prince Sattam Bin Abdulaziz University, Al-Kharj 11942, Saudi Arabia
[4] Civil Engineering Department, Cairo University, Cairo 12613, Egypt; ahmad.202211075@eng-st.cu.edu.eg
[5] Department of Civil Engineering, Faculty of Engineering, Jordan University of Science and Technology, Irbid 21110, Jordan; omarshehabat2002@gmail.com
* Correspondence: m.abduljaber@ju.edu.jo

Abstract

The depletion of natural aggregates and the rapid increase in construction and demolition waste have intensified the need for sustainable structural materials. Recycled aggregates (RAs) represent a promising alternative; however, their performance under elevated temperatures remains insufficiently investigated. This study examines the combined influence of recycled coarse and fine aggregates (RCFA) replacement ratios and fire exposure on the shear behavior of RC beams. Five replacement levels (0%, 25%, 50%, 75%, and 100%) were considered. A total of forty-five beams (1500 × 150 × 200 mm) were tested at 23 °C, 400 °C, and 600 °C. In addition, a finite element model was developed to validate the experimental findings. The results showed at 23 °C, increasing the RA content led to a moderate reduction in the ultimate shear capacity of approximately 6–10%. Fire exposure significantly aggravated strength degradation, with additional reductions of up to 11% at 400 °C and total losses reaching about 22% at 600 °C compared to the control beam at room temperature. Stiffness deterioration and crack propagation became more pronounced with higher temperatures and replacement ratios due to thermal damage to the cement matrix and interfacial transition zones. Nevertheless, moderate replacement levels (25–50%) maintained acceptable residual shear capacity and improved ductility and energy absorption. Numerical predictions closely matched experimental results, with load differences within 1–5%, confirming the model's reliability.

Keywords: shear behavior; recycled coarse aggregate; recycled fine aggregate; RC; high temperature

Check for updates

Received: 22 February 2026
Revised: 17 March 2026
Accepted: 20 March 2026
Published: 31 March 2026

Copyright: © 2026 by the authors. Licensee MDPI, Basel, Switzerland. This article is an open access article distributed under the terms and conditions of the Creative Commons Attribution (CC BY) license.

1. Introduction

The rapid global increase in the demand for concrete and natural aggregates (NAs) has exerted unprecedented pressure on limited natural resources, making resource depletion a major sustainability challenge in the construction sector [1,2]. Global virgin aggregate production increased from approximately 21 billion tons in 2007 to nearly 50 billion tons in 2017 and is projected to reach about 60 billion tons by 2030. This growth has been accompanied by a significant rise in construction and demolition (C&D) waste, which

accounts for more than one-third of total solid waste in many regions; in Europe alone, annual C&D waste generation exceeds 450 million tons [3,4]. In response, the construction industry has adopted an increasing number of sustainability-oriented strategies and circular economy principles, emphasizing waste recycling and reuse as alternatives to NAs in concrete production [5].

Within this framework, recycled aggregates have transitioned from a niche research topic to a widely adopted construction practice. The global recycled aggregate (RA) market has surpassed USD 9 billion, driven by increased construction activity, stricter environmental regulations, and advances in recycling technologies, with the Asia-Pacific region representing the fastest-growing market due to rapid urbanization and large-scale infrastructure development [6–8]. Recycled aggregates derived from C&D waste, including recycled coarse and fine aggregates (RCAs and RFAs), have therefore emerged as viable alternatives to NAs. RAs provide clear environmental benefits while maintaining acceptable structural performance when designed appropriately [9,10]. However, the presence of adhered old mortar and pre-existing interfacial transition zones (ITZs) results in higher porosity, increased water absorption, and reduced mechanical strength compared to NAs, potentially affecting durability and long-term performance [11,12].

Accordingly, increasing research attention has been directed toward the structural application of RAs, particularly in reinforced concrete (RC) beams. Experimental studies have demonstrated that recycled aggregate content significantly influences shear behavior. Etman et al. [13] reported progressive reductions in shear capacity with increasing RCA replacement, with failure load decreases ranging from 6.9% to 20.3% for replacement ratios between 25% and 100%. Similarly, Mahmoud et al. [14] observed that combined RCA and RFA replacement caused more pronounced shear capacity reductions, reaching approximately 30% at full replacement, accompanied by wider diagonal cracking and increased splitting along the tension reinforcement. These findings indicate that shear resistance is highly sensitive to both the type and proportion of RA. Moreover, several studies have shown that recycled fine aggregates exert a more detrimental effect on shear performance than recycled coarse aggregates alone. Wardeh and Ghorbel [15] reported reductions in shear strength of up to 20% for beams incorporating high RFA contents or 100% recycled aggregate concrete (RAC). Nevertheless, performance improvements have been achieved through enhancement techniques. Mathew et al. [16] demonstrated that pre-treatment of RCAs combined with steel fiber reinforcement increased shear capacity by approximately 20% and altered the failure mode from shear to flexural. Likewise, Gao et al. [17] showed that incorporating 1.0% steel fibers recovered up to 90% of the shear strength lost due to high ratios of RCA and RFA replacement, while Hossain et al. [18] reported improved ductility despite some reduction in ultimate shear strength.

Although the above-mentioned studies clarify the role of RCAs and RFAs, as well as strengthening techniques, in governing shear performance under normal conditions, the behavior of such beams may be markedly different when subjected to fire exposure. Fire hazards pose a critical risk to buildings, as they can lead to sudden structural degradation and significant material and economic losses [19–26]. Lin et al. [27] reported that RAs exhibited lower spalling frequency and better thermal stability than normal aggregate concrete at temperatures between 600 °C and 800 °C, retaining more residual compressive strength. Similarly, Zhang et al. [28] showed that basalt fiber reinforcement improved the residual compressive strength of RCA concrete by approximately 20% at 600 °C. Nevertheless, significant strength degradation at elevated temperatures has been consistently reported, particularly above 400–600 °C, as confirmed by Amin et al. [29] and Abedalqader et al. [30]. Additionally, Zheng et al. [31] reported shear strength reductions of approximately 20% and 35% for reinforced RAC (RRAC) beams exposed to temperatures of

400 °C and 600 °C, respectively, accompanied by notable stiffness degradation, while Song et al. [32] highlighted severe losses in residual shear capacity for beams without stirrups after prolonged fire exposure. These findings suggest that fire exposure plays a critical role in residual shear performance, yet the combined effects of RCA and RFA contents remain insufficiently explored.

In parallel with experimental investigations, numerical modeling has been employed to elucidate the behavior of RA and RRAC. Yu et al. [33] demonstrated through mesoscale simulations that the tensile properties of RA are governed by the quality of the old mortar and ITZs. Zheng et al. [31] developed finite element models capable of accurately simulating the coupled thermal and shear behavior of RRAC beams, revealing that existing shear design provisions tend to underestimate the residual shear capacity at temperatures below 500 °C. Despite the growing body of experimental and numerical research on RA, studies addressing the shear performance of RC beams incorporating both RCA and RFA after fire exposure remain very limited. Moreover, most existing investigations lack a systematic assessment of the combined effects of varying RCA and RFA contents on residual shear capacity, stiffness degradation, and failure mechanisms. In addition, finite element analysis (FEA) of such systems remains insufficiently explored. Therefore, a comprehensive experimental and numerical study is required to clarify the coupled effects of RA replacement and fire exposure on the shear behavior of RC beams, thereby providing reliable data to support design practice and promote the safe use of RAs in sustainable structural applications.

2. Materials

2.1. Cement

Ordinary Portland cement (CEM II/B-P 42.5 N) (Lafarge Holcim, Amman, Jordan) was employed as the primary binder in this investigation. The cement met the requirements of EN 1994-1-2 [34], ensuring reliable and consistent performance throughout the experimental program. The chemical composition of the cement is presented in Table 1.

Table 1. Chemical composition of cement.

Fe_2O_3	MnO	TiO_2	CaO	K_2O	P_2O_5	SiO_2	Al_2O_3	MgO	Na_2O	SO_3	SG
4.49	<0.022	0.96	56	0.71	0.75	21.6	6.4	2.1	0.99	3.2	3.01

2.2. Coarse and Fine Aggregates

The recycled coarse and fine aggregates used in this study were produced from crushed high-strength concrete that had a compressive strength of about 55 MPa and sufficient maturity at the time of crushing, which contributed to the quality of the resulting recycled aggregates (illustrated in Figure 1). The concrete waste was mechanically crushed in stages to obtain suitable aggregate sizes, after which the material was separated into RCAs and RFAs by sieving. The particle size distributions of both the RCAs and RFAs were determined using standard sieve analysis, and the corresponding grading curves are illustrated in Figure 2. Owing to the high strength and good quality of the parent concrete, the recycled aggregates exhibited relatively low water absorption and satisfactory mechanical performance compared with recycled aggregates sourced from lower-strength concrete. The key physical and mechanical properties of the natural CA (NCA), natural FA (NFA), RCAs, and RFAs are summarized in Table 2.

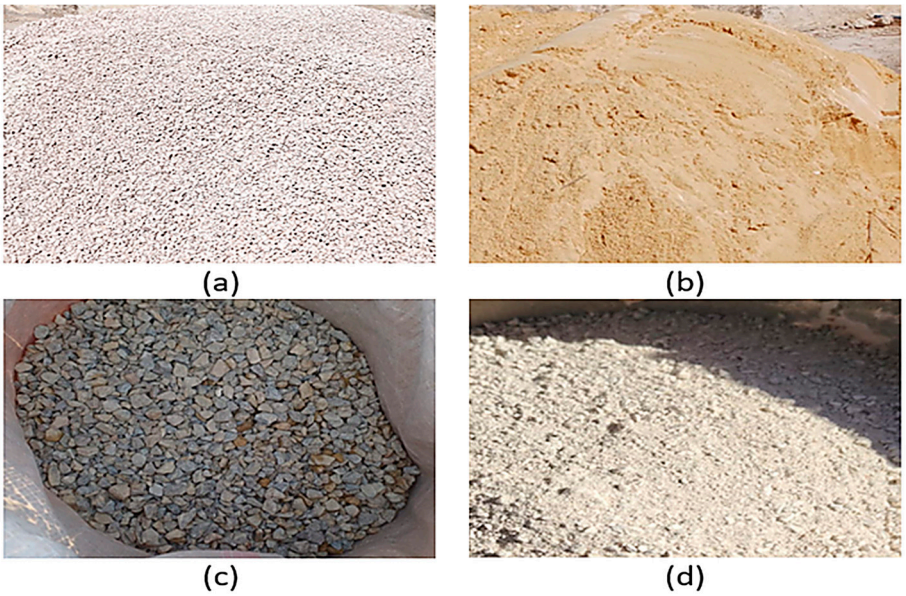


Figure 1. Aggregate: (**a**) NCA; (**b**) NFA; (**c**) RCA; (**d**) RFA.

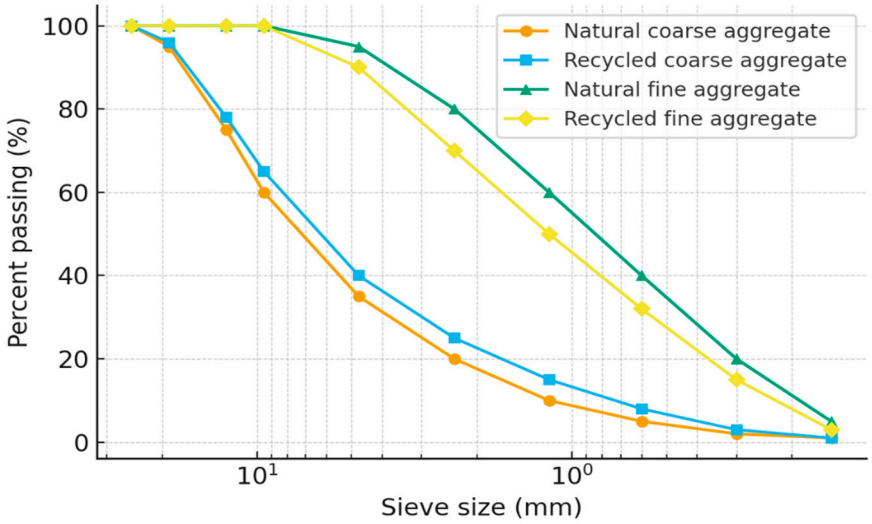


Figure 2. Aggregate gradation.

Table 2. Characteristics of natural and recycled aggregates.

Property	NCA	NFA	RCA	RFA
Bulk density (SSD)	2.23 g/cm^3	2.21	2.19 g/cm^3	2.2 g/cm^3
Specific gravity (OD)	2.58	2.54	2.45	2.47
Water absorption	1.82%	2.88%	2.38%	4.73%
Abrasion	33.6%	-	35.8%	-
Fineness modulus	-	2.72	-	2.37

2.3. Steel Reinforcement

All specimens were reinforced using deformed steel bars. The longitudinal reinforcement consisted of three 16 mm diameter bars placed at the bottom layer and two 10 mm diameter bars at the top, with an average yield strength of 420 MPa. Shear reinforcement was provided in the form of 8 mm diameter closed stirrups with an average yield strength of 280 MPa, spaced at 200 mm along the span.

2.4. Superplasticizer

Conplast SP430 (Fosroc, Amman, Jordan) was employed as a high-range water-reducing admixture to enhance the fresh and hardened properties of the concrete mixtures. The admixture facilitated a reduction in the water content while maintaining adequate workability, which contributed to improved strength development. Its use was particularly effective in mixtures incorporating recycled aggregates, where higher water demand and workability-related challenges are typically observed.

3. Experimental Work

3.1. Mix Proportions

The concrete mixtures were proportioned to investigate the effect of RAs on the shear behavior of RC beams. Five mixtures were prepared in total. The first mixture was used as the control mix and contained only NCA and FCA with zero replacement, with a target compressive strength of 25 MPa. The remaining four mixtures were produced by simultaneously replacing NCA and FCA with RCAs and RFAs at replacement levels of 25%, 50%, 75%, and 100%. All mixtures were designed with the same cement content and water-to-cement ratio to ensure comparable conditions. Nine reinforced concrete beams were cast from each mixture. The detailed mix proportions are summarized in Table 3.

Table 3. Concrete mix proportions.

Mix ID	Replacement Ratio	Cement (kg/m^3)	Water (kg/m^3)	NCA (kg/m^3)	RCA (kg/m^3)	NFA (kg/m^3)	RFA (kg/m^3)	Superplasticizer (L/m^3)
Mix 1	0%	300	150	1060	0	650	0	4.2
Mix 2	25%	300	150	795	265	487.5	162.5	4.2
Mix 3	50%	300	150	530	530	325	325	4.2
Mix 4	75%	300	150	265	795	162.5	487.5	4.2
Mix 5	100%	300	150	0	1060	0	650	4.2

3.2. Beam Details

Forty-five RC beams were designed in accordance with ACI 318-19 [35] to ensure shear-controlled failure. All beams were cast with identical geometric dimensions: a span length of 1500 mm, a width of 150 mm, and a depth of 200 mm. The beams were cast in wooden molds in three layers and compacted using an electric vibrator (Ubuy, Amman, Jordan) to eliminate air voids, after which the top surfaces were finished with a trowel. The specimens were demolded after 24 h and cured for 28 days, during which time they were wrapped with damp burlap and sprayed with water daily. The beam geometry, reinforcement arrangement, and cross-sectional details are presented in Figure 3. In addition, a total of forty-five concrete cubes were cast to evaluate the compressive strength of the concrete mixtures. The cube specimens were cast in three layers to ensure proper compaction, in accordance with ASTM C192/C192M [36].

The beam specimens were classified into three groups based on the investigated temperature levels, namely room temperature, 400 °C, and 600 °C. Each group consisted of fifteen reinforced concrete (RC) beams and fifteen concrete cubes. The specimens were distributed across five replacement ratios (0%, 25%, 50%, 75%, and 100%), with three beams and three concrete cubes tested for each ratio to ensure the reproducibility and reliability of the experimental results. For the elevated temperature groups, the specimens were first exposed to the target temperature and then allowed to cool naturally to ambient conditions, after which mechanical tests were conducted to evaluate the residual structural

capacity after fire exposure. Figure 4 illustrates the casting and curing procedures, while the experimental test matrix is presented in Figure 5.

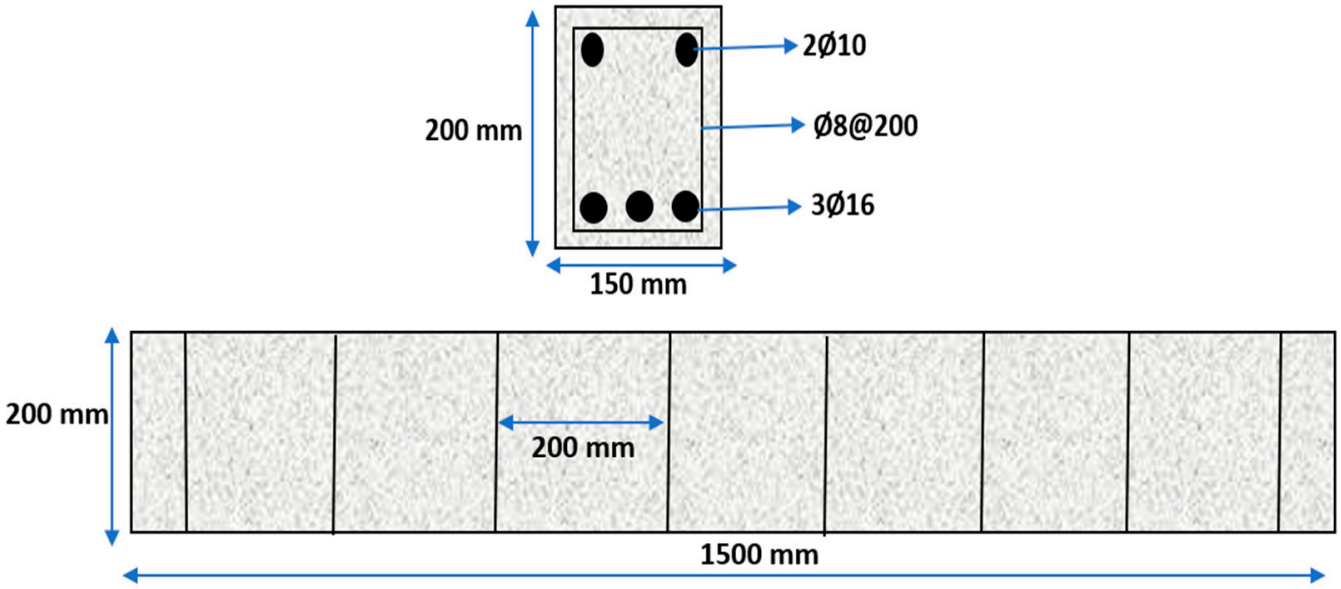


Figure 3. Beam geometry.



Figure 4. Casting and curing process.

Test Matrix	Group 1: 23 °C	0%	3 beams and 3 cubes
		25%	3 beams and 3 cubes
		50%	3 beams and 3 cubes
		75%	3 beams and 3 cubes
		100%	3 beams and 3 cubes
	Group 2: 400 °C	0%	3 beams and 3 cubes
		25%	3 beams and 3 cubes
		50%	3 beams and 3 cubes
		75%	3 beams and 3 cubes
		100%	3 beams and 3 cubes
	Group 3: 600 °C	0%	3 beams and 3 cubes
		25%	3 beams and 3 cubes
		50%	3 beams and 3 cubes
		75%	3 beams and 3 cubes
		100%	3 beams and 3 cubes

Figure 5. Test matrix.

3.3. Heating Procedure

The heating exposure program comprised two elevated temperature levels. The temperatures 400 °C and 600 °C were selected because they represent two widely recognized fire-damage levels. The temperature of 400 °C corresponds to moderate fire exposure, where dehydration of cement hydrates and initial microcracking begin to occur, leading to noticeable reductions in mechanical properties. In contrast, 600 °C represents severe thermal exposure, where significant decomposition of hydration products such as $Ca(OH)_2$ and partial degradation of C–S–H gel occur, accompanied by extensive microcracking and substantial strength deterioration. Therefore, selecting these two temperatures facilitates the evaluation of structural performance under moderate and severe fire-damage conditions. Similar temperature levels have been widely adopted in previous fire-exposure studies on concrete [22–24]. Fifteen reinforced concrete beams were heated to 400 °C, while another fifteen beams were exposed to 600 °C using an electric furnace (Middle East Technology, Amman, Jordan) with internal dimensions of 2.0 m × 1.5 m × 0.6 m. The heating rate was controlled at 5 °C/min, and the furnace temperature was continuously monitored using a digital temperature measurement system to ensure uniform thermal exposure across specimens. The target temperature refers to the furnace air temperature, and the specimens were maintained at the target temperature for 3 h after the furnace reached the specified temperature, ensuring consistent thermal exposure for all specimens.

After completion of the heating duration, all specimens were removed from the furnace and allowed to cool naturally in air to ambient temperature under identical environmental conditions. This cooling approach was adopted to avoid any influence from residual furnace heat and to ensure comparable post-heating conditions for all beams. The heating and cooling procedures are illustrated in Figure 6.

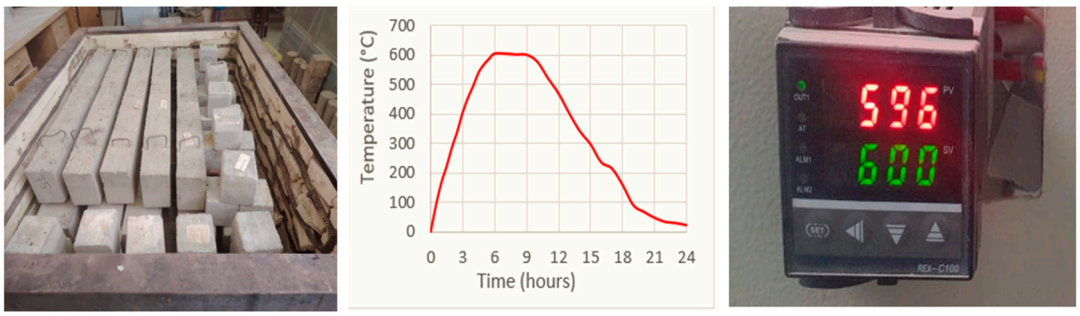


Figure 6. Heating process.

3.4. Test Setup

Forty-five RC beams were experimentally investigated under two-point bending, as shown in Figure 7. All specimens were simply supported to replicate realistic structural behavior. The load was applied through a hydraulic jack with a maximum capacity of 700 kN and was incrementally increased at a constant rate of 5 kN until ultimate failure occurred. Vertical deflections were measured using three LVDTs (Local supplier, Amman, Jordan), with one placed at the midspan of the beam and two positioned symmetrically under the loading points. All measurement channels, including load and displacement readings, were continuously recorded during the test using a digital data acquisition system.

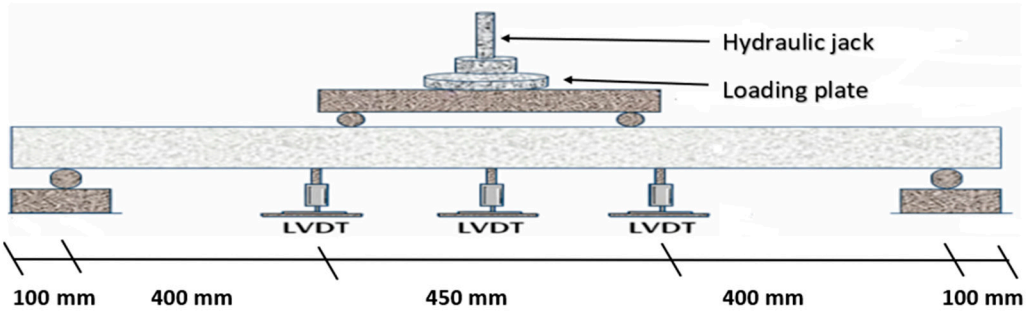


Figure 7. Test setup. (Adapted from [26]).

4. Experimental Results and Discussion

This section presents and discusses the experimental results obtained from evaluating the shear performance of RC beams incorporating varying proportions of RCAs and RFAs before and after fire exposure. The effects of elevated temperature and aggregate replacement ratio on load capacity, stiffness degradation, crack development, and failure modes are systematically examined.

4.1. Compressive Strength

Table 4 presents the average compressive strength values for all tested groups at different temperature levels. At 23 °C, a progressive reduction in compressive strength was observed with an increasing substitution ratio, highlighting the influence of recycled aggregates on the mechanical performance of the concrete mixes. After exposure to elevated temperatures, all mixes exhibited additional strength loss relative to the reference condition at 23 °C. At 400 °C, the compressive strength reduction ranged from 2.6% to 9.4%, which can be attributed mainly to the evaporation of free and physically bound water and the initiation of microcracking resulting from thermal incompatibility between the cement paste and aggregates. Although the cement matrix remains partially stable at this temperature, degradation of the interfacial transition zone reduces stress transfer efficiency, leading to moderate strength loss. A more pronounced deterioration was recorded after exposure to 600 °C, where compressive strength reductions increased significantly, reaching values between 4.7% and 22.1% compared to 23 °C. This behavior is primarily associated with the dehydration of calcium silicate hydrate and the decomposition of calcium hydroxide, which induce severe microstructural damage, increased porosity, and extensive cracking within the concrete matrix. The higher reduction percentages observed in mixes with higher substitution ratios indicate that recycled aggregates are more susceptible to thermal damage due to their higher porosity, the presence of adhered old mortar, and weaker interfacial bonding. Consequently, thermally induced cracks propagate more rapidly in these mixes, accelerating strength degradation.

Table 4. Average compressive strength at different temperatures.

Mix ID	Avg F′cu at 23 °C (MPa)	Avg F′cu at 400 °C (MPa)	Avg F′cu at 600 °C (MPa)
Mix 1, 0%	27.3 ± 1.44	26.4 ± 0.49	24.9 ± 0.22
Mix 2, 25%	25.2 ± 0.89	24.5 ± 0.92	24 ± 0.91
Mix 3, 50%	24.1 ± 0.92	21.8 ± 1.66	20.9 ± 1.24
Mix 4, 75%	23 ± 0.94	20.9 ± 0.7	17.9 ± 0.79
Mix 5, 100%	20.4 ± 1.13	18.9 ± 0.64	17.2 ± 0.94

These results are consistent with previous studies while showing comparatively improved performance. Abedalqader et al. [30] reported compressive strength reductions of approximately 20–27% at 400 °C and up to 37–44% at temperatures between 400 °C and 500 °C for mixes with high recycled aggregate contents. Similarly, Vieira et al. [37] and Chen et al. [38] observed strength losses exceeding 40% for concretes incorporating 60–100% recycled aggregates after elevated temperature exposure. In contrast, the maximum reduction recorded in the present study did not exceed 22.12% at 600 °C, with several mixes exhibiting reductions below 15%. Guo et al. [39] reported that both cube and axial compressive strengths decrease as the replacement ratio of RCAs and RFAs increases. However, no significant reduction was observed for RFA replacement up to 30%. Full replacement of natural aggregates markedly deteriorated the mechanical properties of RAC. Nevertheless, concrete containing 100% RCAs and 60% RFAs at a W/C ratio of 0.4 achieved a compressive strength of 25.37 MPa, which remains adequate for low-grade applications. This enhanced performance is attributed to the use of recycled aggregates sourced from high-strength parent concrete, which provided denser adhered mortar and improved interfacial transition zone characteristics, thereby mitigating thermally induced damage. The relatively low standard deviation values reported in Table 4 further confirm the good repeatability and reliability of the experimental results.

4.2. Load Deflection Curves

Figures 8–10 illustrate the average load–deflection curves of the tested RC beams incorporating different recycled coarse and fine aggregate (RCFA) replacement ratios at room temperature, 400 °C, and 600 °C, respectively. Mid-span deflection was recorded throughout the loading process. As shown in these figures, the load–deflection envelopes corresponding to lower temperature levels consistently surround those obtained at higher temperatures, indicating that exposure to elevated temperatures leads to a noticeable degradation in the shear performance of the beams. This behavior is reflected in reductions in both the ultimate load capacity and the secant stiffness with increasing temperature and RCFA content. At room temperature, the control beam NA-0% exhibited the highest ultimate load of approximately 91.0 kN with a peak deflection of 3.4 mm, whereas beams incorporating RCFAs showed slightly lower ultimate loads ranging between 82.4 kN and 85.2 kN, accompanied by higher peak deflections reaching up to 6.4 mm. After exposure to 400 °C, all beams experienced a reduction in stiffness and load-carrying capacity, with ultimate loads decreasing to values between 73.7 kN and 87.4 kN and peak deflections varying from 3.7 mm to 4.3 mm. A more pronounced degradation was observed after exposure to 600 °C, where the ultimate load further decreased to the range of 70.5 kN to 82.1 kN, while the peak deflection increased significantly, reaching up to 7.0 mm for beams with higher RCFA replacement ratios.

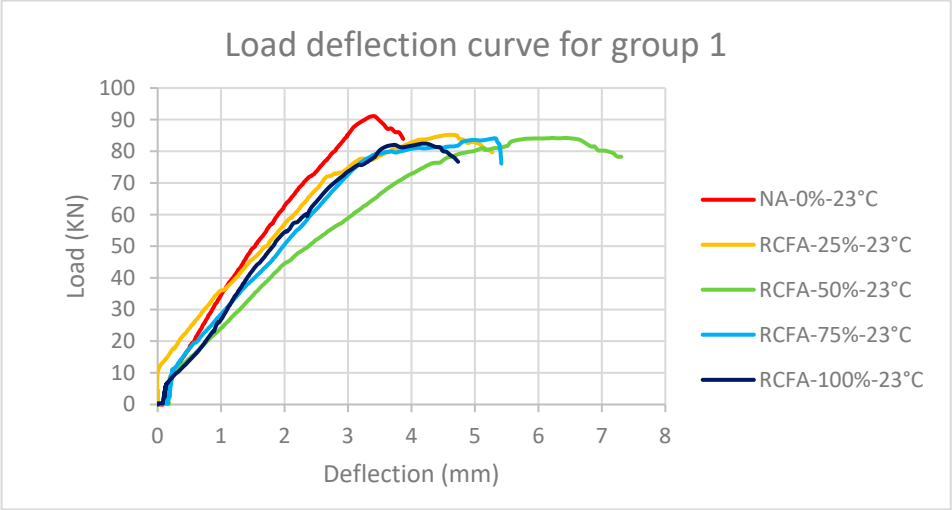


Figure 8. Load-deflection curves of tested beams in group 1.

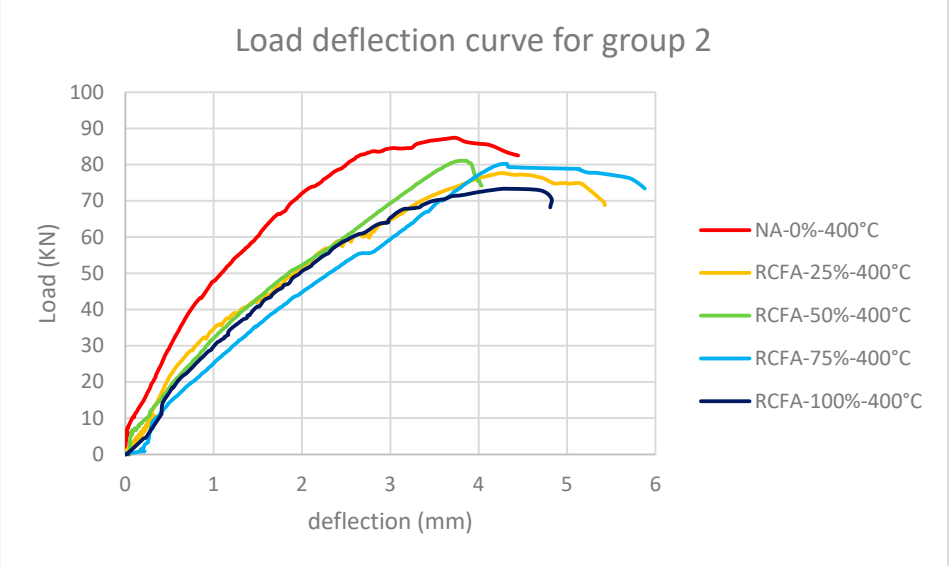


Figure 9. Load-deflection curves of tested beams in group 2.

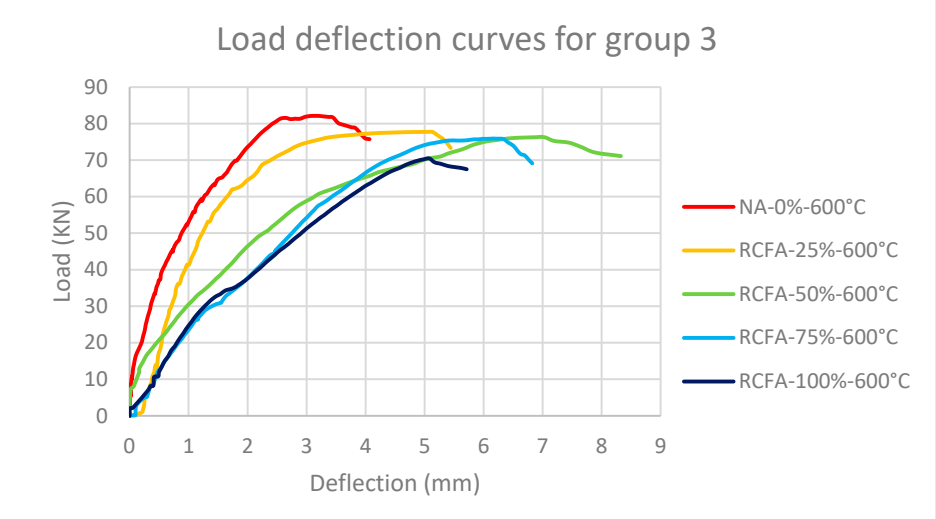


Figure 10. Load-deflection curves of tested beams in group 3.

Three distinct phases can be identified in the load–deflection response of all tested beams. The first phase corresponds to the initial elastic stage, characterized by a nearly linear relationship between load and mid-span deflection up to the elastic limit. The second phase begins beyond this point and is marked by a nonlinear increase in load accompanied by a more rapid increase in deflection, leading to the maximum load capacity. In this phase, beams tested at room temperature and 400 °C exhibited relatively flatter slopes near the peak load, indicating limited gains in load-bearing capacity. The third phase is characterized by a gradual reduction in load with a continuous increase in deflection, reflecting stiffness degradation and damage accumulation. The reduced slope of the curves at elevated temperatures, particularly at 600 °C, highlights the significant thermal damage sustained by the concrete matrix, the RCFA particles, and the steel reinforcement, resulting in diminished stiffness and increased deformability.

4.3. Ultimate Load

Figure 11 and Table 5 illustrates the effect of the recycled coarse fine aggregate RCFA replacement ratio and exposure temperature on the ultimate load capacity of the tested RC beams. At an ambient temperature of 23 °C, the control beam NA-0% exhibited the highest ultimate load of 91.0 kN. The incorporation of RCFAs led to a moderate reduction in load-carrying capacity, with ultimate loads of 85.2 kN, 84.3 kN, 84.1 kN, and 82.4 kN for replacement ratios of 25%, 50%, 75%, and 100%, respectively. This corresponds to a reduction of approximately 6.4% to 9.5% relative to the control beam, indicating that increasing the RCFA content slightly influences the ultimate load under room-temperature conditions. After exposure to 400 °C, all beams exhibited a further decline in ultimate load capacity. The NA-0% beam retained an ultimate load of 87.4 kN, while beams incorporating RCFAs recorded values ranging from 81.5 kN at 25% replacement to 73.7 kN at 100% replacement. Compared with their corresponding ambient-temperature specimens, the reduction in ultimate load ranged from approximately 4% to 11%, reflecting the combined effects of thermal damage and RCFA incorporation on shear resistance.

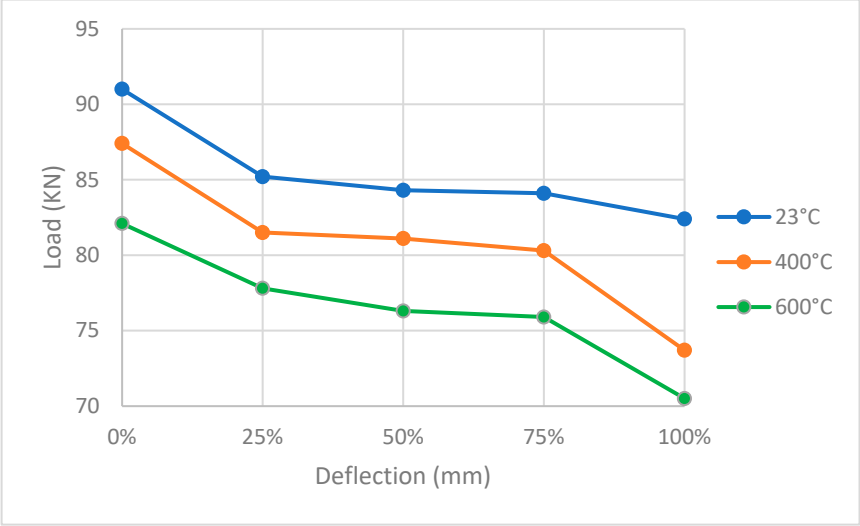


Figure 11. Effect of RCFA replacement ratio and exposure temperature on ultimate load.

A more pronounced degradation was observed after exposure to 600 °C. The ultimate load of the control beam decreased to 82.1 kN, whereas beams containing RCFAs exhibited ultimate loads of 77.8 kN, 76.3 kN, 75.9 kN, and 70.5 kN for replacement ratios of 25%, 50%, 75%, and 100%, respectively. This represents a maximum reduction of about 22.5% relative to the control beam tested at ambient temperature. Overall, the results demonstrate that

increasing RCFA replacement ratios amplify the detrimental effect of elevated temperature on ultimate load capacity. This behavior is attributed to thermally induced microcracking, degradation of the concrete matrix, and weakening of the interfacial transition zone, which collectively reduce the ability of the beams to sustain high shear loads.

Table 5. Ultimate load and peak deflection for RC beams.

Beam ID	Mean Ultimate Load (kN)	Mean Peak Deflection (mm)
NA-0%	91.0	3.4
RCFA-25%	85.2	4.6
RCRA-50%	84.3	6.4
RCRA-75%	84.1	5.3
RCFA-100%	82.4	4.2
NA-0%-400 °C	87.4	3.7
RCFA-25%-400 °C	81.5	4.3
RCFA-50%-400 °C	81.1	3.9
RCFA-75%-400 °C	80.3	4.3
RCFA-100%-400 °C	73.7	4.2
NA-0%-600 °C	82.1	3.2
RCFA-25%-600 °C	77.8	5.1
RCFA-50%-600 °C	76.3	7.0
RCFA-75%-600 °C	75.9	6.0
RCFA-100%-600 °C	70.5	5.1

4.4. Failure Mode

The tested beams were designed to fail in shear, and the observed damage patterns were consistent with classical diagonal shear behavior. As shown in Figure 12, initial flexural cracks appeared at the tension zone near mid-span and progressively extended toward the shear spans. These cracks subsequently developed into inclined shear cracks propagating toward the loading points and supports. At ambient temperature, the control beam NA-0% exhibited first cracking at 18 kN, while beams incorporating RCFAs showed first-crack loads ranging between 12 and 21 kN depending on the replacement ratio. Although the crack initiation load varied slightly with the RCFA content, the overall crack progression followed a similar pattern characterized by flexural cracking followed by the formation of dominant diagonal shear cracks. After exposure to 400 °C, crack development became more pronounced. First cracking occurred between 12 and 19 kN, and inclined shear cracks formed earlier within the shear span compared to specimens tested at ambient temperature. The cracks appeared wider and more distributed, reflecting thermally induced microcracking and partial degradation of the concrete matrix. At 600 °C, crack propagation was more rapid and severe. First-crack loads ranged between 14 and 20 kN, and multiple inclined cracks developed before merging into a critical diagonal crack leading to failure. The images clearly show increased crack density and wider crack openings, particularly in beams with higher RCFA replacement ratios. Thermal exposure intensified the weakening of the interfacial transition zone and reduced aggregate interlocking, accelerating crack growth within the shear span. These results are consistent with the findings of Chen et al. [40], who reported that RAC maintained comparable mechanical performance up to 400 °C, while significant deterioration occurred at 600 °C due to thermal decomposition

of cement hydrates and increased internal cracking after water cooling. The damage was primarily attributed to the decomposition of Ca $(OH)_2$ into CaO at high temperatures and its subsequent rehydration, leading to internal expansion and microcrack propagation, while preserving a similar overall failure pattern characterized by more pronounced cracking and reduced load-carrying capacity at elevated temperatures.

Overall, while increasing the RCFA content and exposure temperature influenced crack initiation and propagation characteristics, diagonal shear cracking remained the predominant failure mechanism. The similarity in crack patterns across all specimens indicates that temperature and recycled aggregate content primarily affected crack development intensity rather than altering the fundamental shear failure mode.



Figure 12. *Cont.*

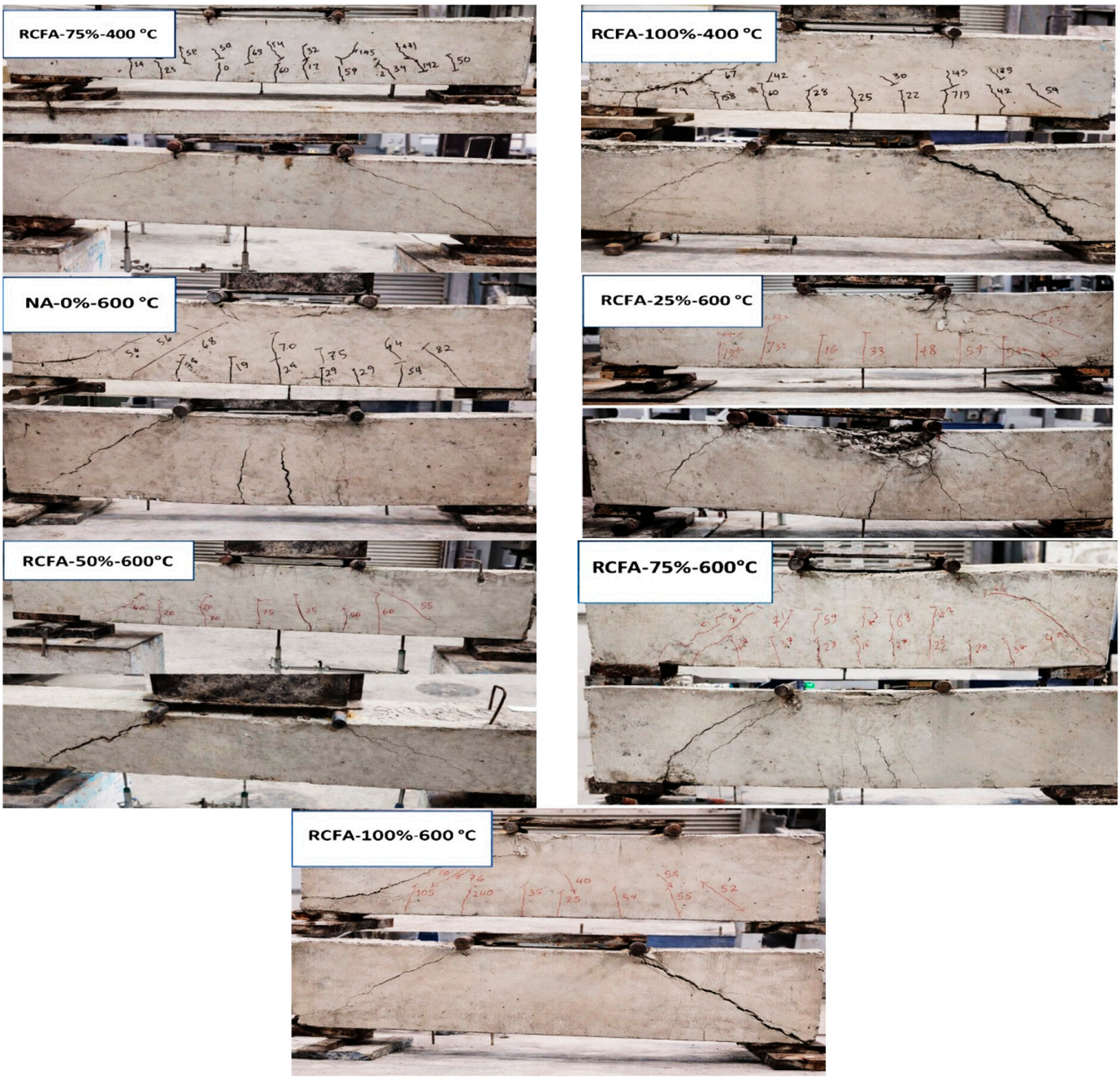


Figure 12. Failure modes of beams.

4.5. Stiffness

The stiffness values derived from the load–deflection curves, as summarized in Table 6, reveal clear differences among the tested beam groups. The initial stiffness was calculated from the slope of the linear portion of the load–deflection curve ($\Delta P/\Delta\delta$), representing the elastic response of the beam prior to significant cracking. This method enabled a consistent comparison of stiffness behavior for specimens subjected to different RCFA replacement ratios and temperature exposure levels. At ambient temperature, the control beam exhibited the highest initial stiffness of 26.9 kN/mm, while beams incorporating recycled coarse and fine aggregates generally showed lower stiffness values. The lowest stiffness was observed at 50% RCFA replacement (13.2 kN/mm), indicating increased deformability associated with the presence of recycled aggregates. This reduction can be attributed to the higher porosity, pre-existing microcracks, and weaker interfacial bonding

typically associated with recycled aggregates, which promote earlier crack initiation and greater deformation under loading. Following exposure to elevated temperatures, stiffness degradation became more evident. At 400 °C, stiffness values remained within a relatively narrow range, with the control beam maintaining the highest stiffness (23.5 kN/mm), while beams incorporating recycled aggregates exhibited slightly lower values. However, at 600 °C, the reduction became more pronounced, particularly for beams containing recycled aggregates. The beam with 50% RCFA replacement showed the lowest stiffness value (10.9 kN/mm), reflecting the combined effects of thermal microcracking, deterioration of the cement matrix, and weakening of the aggregate–paste bond.

Table 6. Statistical summary of stiffness values for all beam groups.

Beam ID	Mean Stiffness (kN/mm)	SD	COV (%)
NA-0%	26.9	0.61	2.3
RCFA-25%	18.5	0.43	2.3
RCFA-50%	13.2	0.26	2
RCFA-75%	16.9	0.32	2
RCFA-100%	19.7	0.71	3.6
NA-0%-400 °C	23.5	0.63	2.7
RCFA-25%-400 °C	19	0.49	2.6
RCFA-50%-400 °C	20.8	0.44	2.1
RCFA-75%-400 °C	18.8	0.55	2.9
RCFA-100%-400 °C	17.6	0.28	1.6
NA-0%-600 °C	25.7	0.59	2.3
RCFA-25%-600 °C	15.2	0.15	1
RCFA-50%-600 °C	10.9	0.44	4
RCFA-75%-600 °C	12.7	0.15	1.2
RCFA-100%-600 °C	13.9	0.24	1.7

Overall, the results indicate that stiffness is influenced by both recycled aggregate content and temperature exposure. While the incorporation of recycled aggregates generally increases beam deformability compared with the control specimen, elevated temperature appears to be the dominant factor governing stiffness degradation, primarily due to thermal microcracking and progressive deterioration of the concrete matrix. These findings are consistent with the observations of Zheng et al. [31], who reported that increasing the percentage of RCA replacement leads to a reduction in the initial stiffness of recycled aggregate concrete beams due to the lower toughness of recycled aggregates and the presence of pre-existing microcracks generated during the crushing process.

4.6. Ductility and Energy Absorption

The load–deflection curves presented in Figures 8–10 demonstrate noticeable variations in ductility and energy absorption associated with the observed failure modes. The ductility ratio (μ) was calculated as the ratio between the peak deflection (δu) and the first-crack deflection (δcr) obtained from the load–deflection curves, while the energy absorption capacity was evaluated as the area under the load–deflection curve up to the peak load. As summarized in Table 7, beams incorporating recycled coarse and fine aggregates generally exhibited comparable or slightly higher deformation capacity than the control beam

at ambient temperature. In particular, the beam with 50% RCFA replacement exhibited the highest ductility ratio (μ = 7.03), whereas the control beam showed a lower value of μ = 5.06, indicating a more localized cracking pattern and a relatively brittle shear response. After exposure to 400 °C, the ductility ratios remained within a comparable range, varying between 3.89 and 6.72, suggesting that the incorporation of recycled aggregates did not significantly compromise the deformation capacity despite thermal degradation. Within this temperature group, the beam with 75% RCFA replacement exhibited the highest ductility ratio (μ = 6.72). At 600 °C, the influence of temperature became more pronounced, and the control beam exhibited a lower ductility ratio (μ = 4.33), indicating a somewhat more brittle structural response. In contrast, beams containing recycled aggregates maintained a comparable deformation capacity, with ductility ratios ranging between approximately 3.80 and 5.05. The energy absorption capacity, summarized in Table 8, shows a similar trend. At ambient temperature, the beam incorporating 50% RCFA replacement demonstrated the highest energy absorption capacity (269.8 kN·mm), which was considerably higher than that of the control beam (154.7 kN·mm). Comparable behavior was observed at elevated temperatures, where several beams incorporating recycled aggregates exhibited a higher energy dissipation capacity than the control specimen. However, at full replacement levels, the weakening of the interfacial transition zone and the reduced aggregate toughness contributed to earlier localization of diagonal cracking and consequently lower overall toughness.

Table 7. Statistical summary of ductility ratios values for all beam groups.

Beam ID	Mean Ductility Ratio μ	SD	COV (%)
NA-0%	5.06	0.31	5.1
RCFA-25%	5	0.18	3.6
RCFA-50%	7.03	0.51	6.8
RCFA-75%	4.02	0.04	1.1
RCFA-100%	6.89	0.34	4.9
NA-0%-400 °C	5.44	0.37	6.4
RCFA-25%-400 °C	4.3	0.58	8.4
RCFA-50%-400 °C	5.06	0.32	5.9
RCFA-75%-400 °C	6.72	0.36	5.6
RCFA-100%-400 °C	3.89	0.14	3.8
NA-0%-600 °C	4.33	0.27	6.1
RCFA-25%-600 °C	4.86	0.35	7.3
RCFA-50%-600 °C	3.83	0.27	7.2
RCFA-75%-600 °C	3.8	0.32	8.2
RCFA-100%-600 °C	5.05	0.3	6.3

Overall, the results indicate that ductility and energy absorption are closely related to the failure mechanism. Beams exhibiting higher ductility tended to develop more distributed cracking and progressive shear failure, whereas lower ductility values were associated with the sudden formation of dominant diagonal cracks and localized crushing in the compression zone. These observations suggest that the incorporation of recycled aggregates can maintain, and in some cases improve, the deformation capacity and energy dissipation of RC beams, even under elevated temperature conditions.

Table 8. Statistical summary of energy absorption capacity for all beam groups.

Beam ID	Mean Energy Absorption (kN·mm)	SD	COV (%)
NA-0%	154.7	9.4	6.1
RCFA-25%	196	7.3	3.7
RCFA-50%	269.8	19.4	7.2
RCFA-75%	222.9	2.5	1.1
RCFA-100%	173	8.6	5
NA-0%-400 °C	161.7	11	6.8
RCFA-25%-400 °C	175.2	13.5	9.4
RCFA-50%-400 °C	158.1	10.1	6.4
RCFA-75%-400 °C	172.6	9.3	5.4
RCFA-100%-400 °C	154.8	5.6	3.6
NA-0%-600 °C	131.4	8.1	6.2
RCFA-25%-600 °C	198.4	14.1	7.1
RCFA-50%-600 °C	267.1	19	7.1
RCFA-75%-600 °C	227.7	18.9	8.3
RCFA-100%-600 °C	179.8	10.6	5.9

4.7. Statistical Reliability Analysis

As presented in Table 9, statistical reliability analysis was conducted to assess the consistency and dispersion of the experimental results. The mean, standard deviation (SD), and coefficient of variation (COV) were calculated for both ultimate load and peak deflection. For ultimate load, the COV values ranged between 1.0% and 4.0%, indicating excellent experimental stability and minimal variability among repeated measurements. This confirms the reliability of the observed trends related to recycled aggregate replacement and temperature exposure. Regarding peak deflection, most COV values remained below 10%, with only one specimen slightly exceeding this range at 13.4%. Overall, the variability remains within acceptable limits for structural testing of reinforced concrete members. The low dispersion values reported in Table 9 confirm that the differences observed in stiffness, ductility, and load capacity are primarily attributed to the influence of recycled aggregate content and elevated temperature rather than experimental uncertainty.

Table 9. Statistical reliability analysis of RC beams.

Beam ID	Mean Ultimate Load (kN)	SD (Load)	COV (Load) (%)	Mean Peak Deflection (mm)	SD (Def.)	COV (Def.) (%)
NA-0%	91.0	2.07	2.3	3.43	0.21	6.1
RCFA-25%	85.2	1.95	2.3	4.60	0.17	3.7
RCFA-50%	84.3	1.67	2.0	6.37	0.46	7.2
RCFA-75%	84.1	1.70	2.0	5.33	0.06	1.1
RCFA-100%	82.4	2.94	3.6	4.23	0.21	5.0
NA-0%-400 °C	87.4	2.36	2.7	3.67	0.25	6.8
RCFA-25%-400 °C	81.5	2.10	2.6	4.33	0.58	13.4
RCFA-50%-400 °C	80.4	1.70	2.1	3.93	0.25	6.4

Table 9. *Cont.*

Beam ID	Mean Ultimate Load (kN)	SD (Load)	COV (Load) (%)	Mean Peak Deflection (mm)	SD (Def.)	COV (Def.) (%)
RCFA-75%-400 °C	80.3	2.31	2.9	4.27	0.23	5.4
RCFA-100%-400 °C	73.7	1.15	1.6	4.17	0.15	3.6
NA-0%-600 °C	82.1	1.90	2.3	3.20	0.20	6.2
RCFA-25%-600 °C	77.8	0.80	1.0	5.10	0.36	7.1
RCFA-50%-600 °C	76.3	3.03	4.0	7.00	0.50	7.1
RCFA-75%-600 °C	75.9	0.90	1.2	6.00	0.50	8.3
RCFA-100%-600 °C	70.5	1.20	1.7	5.10	0.30	5.9

4.8. Discussion of Experimental Results

4.8.1. Effect of Heating Degree

The influence of elevated temperature on the load-carrying capacity of the tested beams is illustrated in Figure 13, which presents the reduction ratio of ultimate load relative to the corresponding ambient-temperature specimens. The results clearly indicate that increasing the temperature leads to a progressive decline in structural capacity across all replacement ratios. At 400 °C, the reduction in load capacity remained moderate, ranging between 3.8% and 4.5% for replacement ratios of up to 75%, while a more noticeable decrease of 10.6% was recorded at 100% RCFA replacement. This suggests that moderate heating causes limited degradation in concrete strength and bond characteristics, with a more pronounced effect appearing at full replacement with recycled aggregate. In contrast, exposure to 600 °C resulted in significantly higher reductions in load capacity. The reduction ratio ranged from 8.7% to 9.8% for replacement levels between 0% and 75%, and reached 14.4% at 100% replacement. The greater decline at 600 °C can be attributed to severe thermal damage, including microcracking of the cement matrix, deterioration of the interfacial transition zone, and weakening of the bond between reinforcement and concrete.

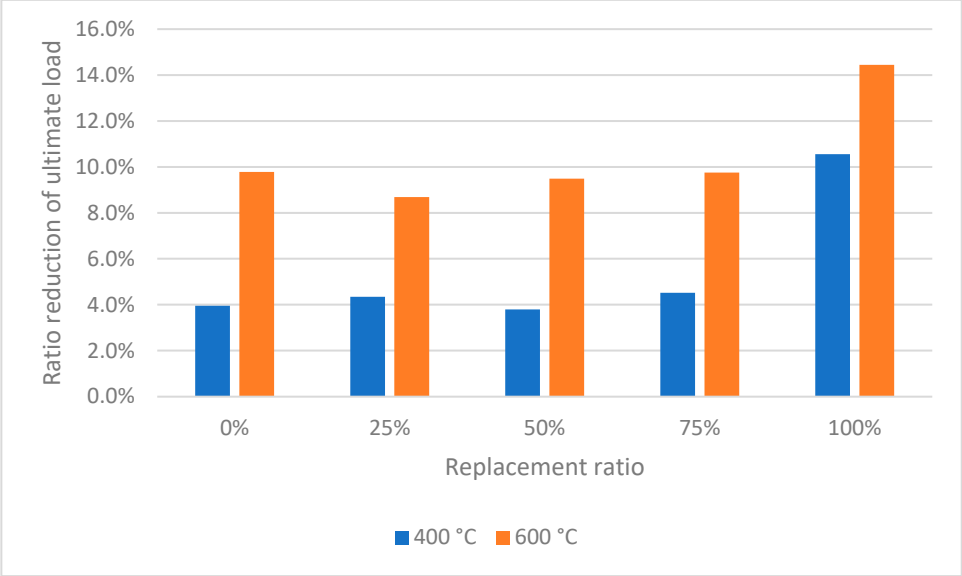


Figure 13. Effect of heating on ultimate load.

These results are consistent with the findings of previous studies [27–31], which indicate that RAC can maintain acceptable performance at moderate temperatures; however,

pronounced deterioration occurs beyond 400–600 °C, with shear strength reductions of approximately 20% at 400 °C and 35% at 600 °C, accompanied by significant stiffness degradation. Overall, the results presented in Figure 13 confirm that temperature is a dominant factor influencing structural performance. While recycled aggregate content slightly amplifies the reduction at high replacement levels, thermal exposure remains the primary cause of capacity degradation, particularly at 600 °C.

4.8.2. Effect of Replacement Ratio

The residual ultimate load ratio, defined as the ratio between the ultimate load of RCFA beams and that of the corresponding control beam at the same temperature level, is illustrated in Figure 14. The results show a gradual reduction in load capacity with an increasing replacement ratio, while the influence of temperature becomes more evident at higher replacement levels. At 23 °C, the residual load ratio decreased progressively from 0.94 at 25% replacement to 0.91 at 100% replacement. This indicates a moderate reduction in load capacity attributed to the weaker interfacial transition zone and higher porosity associated with recycled aggregates, although the structural response remained close to that of the control beam. At 400 °C, the residual ratios for replacement levels up to 75% remained between 0.92 and 0.93, demonstrating limited additional degradation. However, at 100% replacement, the residual ratio dropped significantly to 0.84, reflecting the combined effect of thermal damage and the inherently lower mechanical integrity of pure RAC. At 600 °C, the residual load ratios for moderate replacement levels ranged between 0.92 and 0.95, indicating that partial replacement maintained comparable post-fire performance. Nevertheless, the beam with 100% replacement recorded a residual ratio of 0.86, confirming that high recycled aggregate content amplifies strength reduction under severe thermal exposure. These results are consistent with the findings of Al Mahmoud et al. [14], who reported shear strength reductions ranging from 11% to 19% at 30% recycled aggregate replacement and up to 30% under full replacement while maintaining similar shear failure modes characterized by major diagonal cracking. In addition, Wardeh and Ghorbel [15] observed that full replacement with RFA concrete resulted in shear strength reductions reaching approximately 20% compared to conventional beams. Additionally, Gao et al. [17] reported that as the replacement ratios of RFA and RCA increased, the shear capacity of the concrete beam with RA and steel fibers decreased by 10.43% and 15.52% with increases in the RCA replacement ratio to 50% and 100%. These findings align well with the present results, which show a reduction in shear capacity with increasing recycled aggregate content and temperature without significant alteration in the failure mechanism.

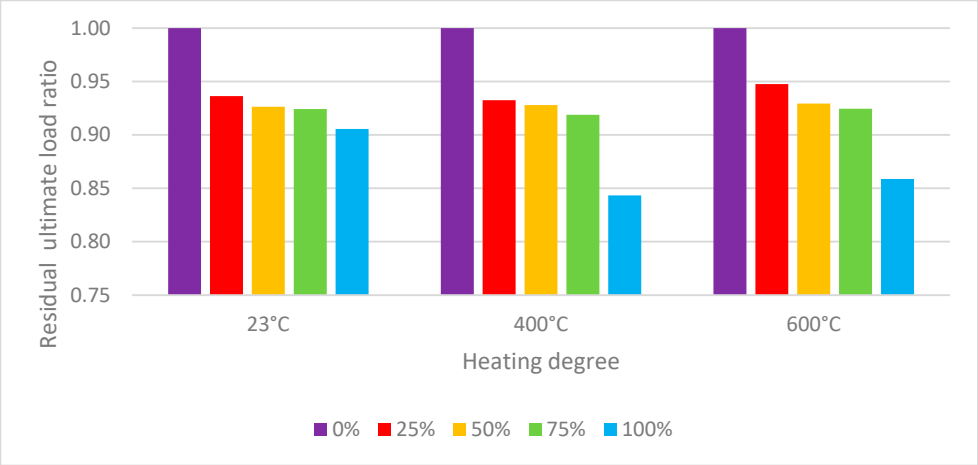


Figure 14. Effect of replacement ratio on ultimate load.

Overall, as shown in Figure 14, moderate RCFA replacement levels keep the residual load capacity within acceptable limits, whereas full replacement leads to a more pronounced reduction, particularly after exposure to elevated temperatures.

5. Finite Element Analysis

5.1. Model Description

A three-dimensional nonlinear finite element model was developed using ABAQUS 2020 to simulate the shear behavior of reinforced concrete beams incorporating recycled aggregates under ambient and elevated temperature conditions. The beam geometry and reinforcement configuration were defined according to the experimental layout illustrated in Figure 3 to ensure full consistency with the tested specimens. Concrete was modeled as a three-dimensional deformable solid using eight-node linear brick elements with reduced-integration C3D8R, while the longitudinal reinforcement and stirrups were represented using two-node linear truss elements in T3D2. Steel loading plates were also included to accurately reproduce the experimental boundary and loading conditions. The overall modeling procedure, including geometry creation, material definition, meshing, interaction assignment, boundary conditions, and loading application, is illustrated in Figure 15.

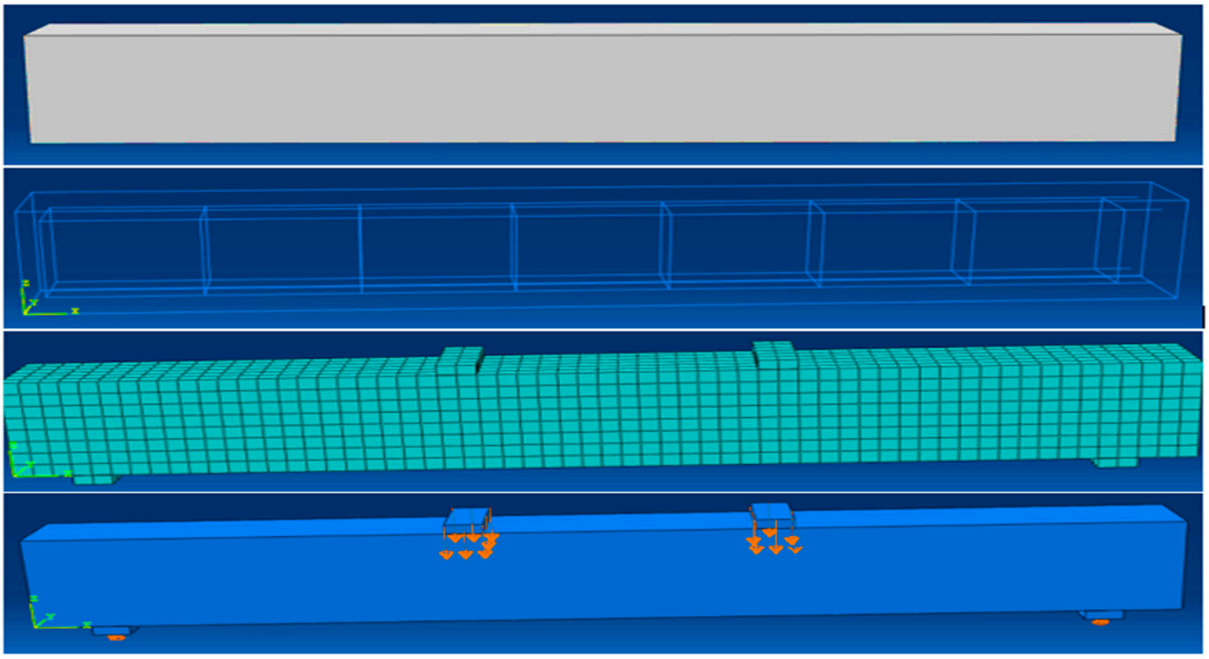


Figure 15. Modeling procedure.

Recent studies have proposed advanced numerical approaches to simulate crack initiation and propagation in heterogeneous quasi-brittle materials. For instance, Choi et al. (2025) [41] developed a cohesive zone-modeling framework capable of capturing complex crack propagation phenomena such as crack branching and coalescence in multiphase composites through adaptive element splitting and cohesive surface elements combined with energy-based crack growth criteria. Similarly, De Maio et al. (2025) [42] introduced an adaptive cohesive interface model combined with a moving mesh technique based on an Arbitrary Lagrangian–Eulerian (ALE) formulation to simulate crack propagation along a priori unknown paths in heterogeneous materials while reducing mesh dependency and remeshing requirements. Compared with these fracture-tracking formulations, the present study employs the Concrete Damage Plasticity (CDP) model in ABAQUS as a

continuum damage approach. Although CDP does not explicitly track individual crack paths, it provides a robust and computationally efficient framework for capturing stiffness degradation, cracking, and the global structural response of reinforced concrete beams.

The nonlinear behavior of concrete was simulated using the Concrete Damage Plasticity (CDP) model available in ABAQUS, in which the compressive and tensile stress–strain relationships were defined based on Tsai's constitutive model to capture tensile cracking and compressive crushing through stiffness degradation parameters. The average compressive strength values were adopted from Table 4. The modulus of elasticity at ambient temperature was calculated based on the empirical relationship $E = 4700 \sqrt{F'_{cu}}$. However, this relationship becomes unreliable at elevated temperatures due to the degradation of the concrete's mechanical properties. Therefore, the reduction in the elastic modulus at 400 °C and 600 °C was determined according to the provisions of EN 1994-1-2 [34]. For mix 1, the elastic modulus was 24,557 MPa at ambient temperature, which decreased to 13,506 MPa at 400 °C and further to 6139 MPa at 600 °C. The elastic modulus values for the remaining concrete mixes were calculated using the same approach, based on their corresponding compressive strength values reported in Table 4. Poisson's ratio of 0.2 was maintained for all temperature levels. The compressive and tensile stress–strain curves used in the model are presented in Figure 16. The tensile behavior was defined by a linear elastic response up to the tensile strength followed by a descending softening branch to represent crack propagation. Concrete stiffness degradation under compression and tension was represented using the damage parameters dc and dt, respectively, which range between 0 (undamaged state) and 1 (complete loss of stiffness). The damage evolution was calculated using the following relationships:

$$dc = 1 - \frac{\sigma c}{f'co} \quad (1)$$

$$dt = 1 - \frac{\sigma t}{f'ct} \quad (2)$$

where σc and σt the compressive and tensile stresses along the descending branch of the stress–strain curves, and f′co and f′ct represent the peak compressive and tensile strengths, respectively. The remaining CDP parameters were defined as follows: dilation angle = 35°; eccentricity = 0.1; biaxial-to-uniaxial compressive strength ratio fb_0/fc_0 = 1.16; stress invariant ratio K = 0.667; viscosity parameter = 0.001. These values are commonly adopted for reinforced concrete modeling in ABAQUS. The steel reinforcement was modeled using a linear elastic–perfectly plastic relationship, with a yield strength and modulus of elasticity of 420 MPa and 200 GPa at ambient temperature, which were reduced to 395 MPa and 112 GPa at 400 °C and further reduced to 168 MPa and 48 GPa at 600 °C to account for thermal degradation [26].

After defining the material properties, the model components were assembled using the Assembly module in ABAQUS. The concrete beam, reinforcement bars, and steel loading plates were positioned according to the experimental configuration to ensure consistency with the test setup. The interaction between the concrete and reinforcement was defined using the embedded region constraint, assuming a perfect bond between the steel reinforcement and concrete without slip. In contrast, the steel loading and support plates were connected to the concrete using tie constraints to ensure proper load transfer and full compatibility at the interface. Next, the analysis step was defined in the Step module with a total duration of 1 s to improve computational efficiency while maintaining numerical stability. All models were analyzed using the same step configuration. Boundary conditions were then applied to represent a simply supported beam configuration. The longitudinal direction of the beam was defined as the *X*-axis, the vertical direction as

the *Y*-axis, and the transverse direction as the *Z*-axis. At the left support, translations in all directions (UX = UY = UZ = 0) were restrained to prevent rigid body motion, forming a pinned support. At the right support, the vertical displacement was restrained (UY = 0) while the horizontal displacements (UX and UZ) were allowed, representing a roller support condition. The load was applied to the nodes located along the centerline of the loading plates to replicate the experimental loading configuration.

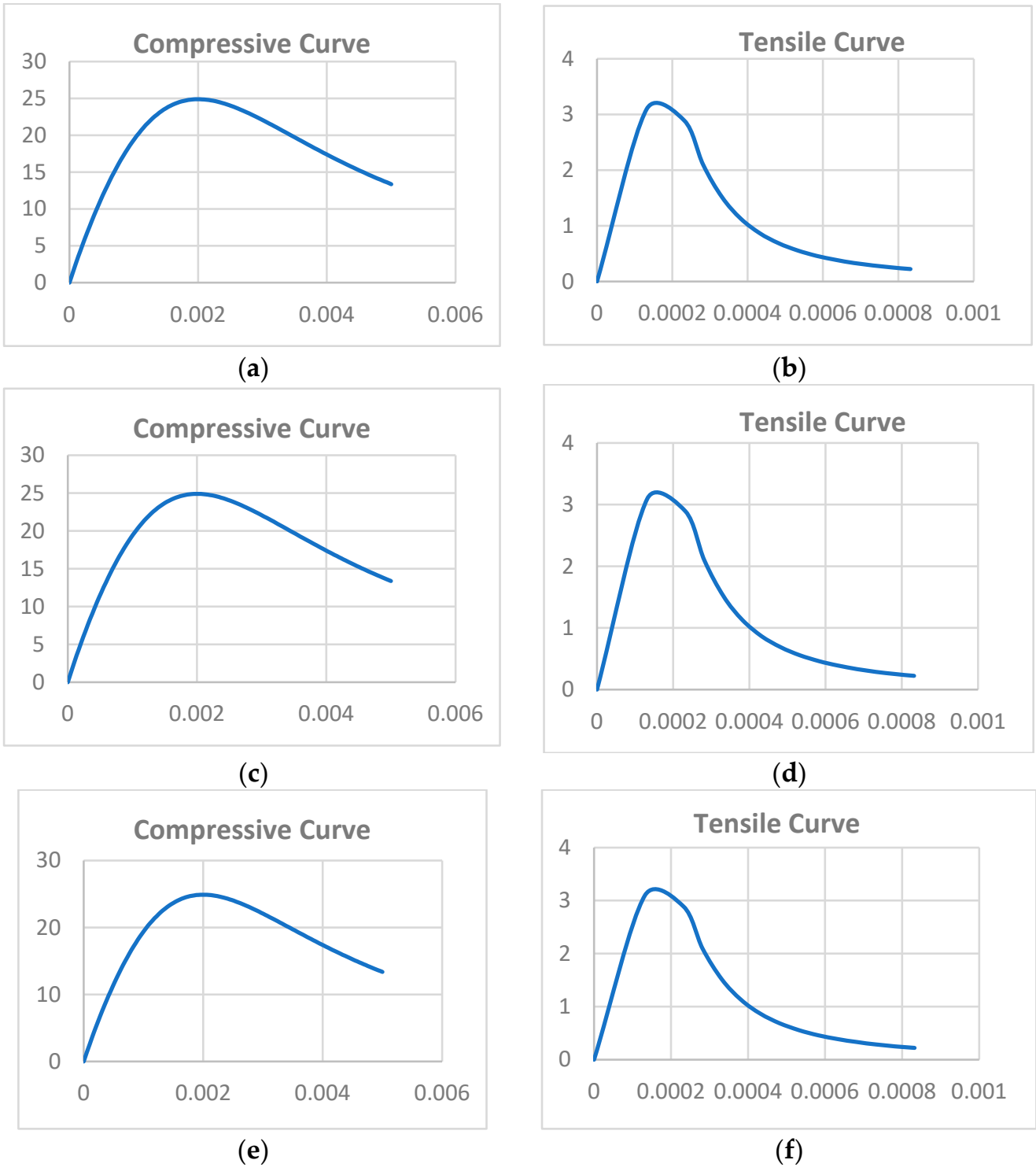


Figure 16. Stress–strain diagram of Mix 1: (**a**) compressive curve at 23 °C; (**b**) tensile curve of at 23 °C; (**c**) compressive curve at 400 °C; (**d**) tensile curve at 400 °C; (**e**) compressive curve at 600 °C; (**f**) tensile curve at 600 °C.

A displacement-controlled loading method was adopted to ensure numerical stability and accurately capture the post-peak structural response. The applied displacement increased gradually in a linear manner throughout this step of the analysis. This approach avoided numerical instability and prevented unrealistic velocity and acceleration effects that may occur when load-controlled procedures are used beyond the peak load. For mesh generation, structured hexahedral elements were employed due to the regular geometry of the beams, which improves element quality and enhances convergence stability during the analysis. A uniform mesh size of 25 mm was adopted for the concrete elements to achieve an appropriate balance between computational efficiency and numerical accuracy. The selected mesh size was based on recommendations reported in previous studies, which indicate that element sizes within a range of approximately 20–50 mm for reinforced concrete beams and slabs generally provide stable numerical results. Within this range, mesh refinement typically results in only minor differences of less than 5% in key response parameters such as ultimate load and mid-span deflection [26,43,44].

Finally, in the Output request module, both field output and history output were defined to monitor the structural response during the analysis. The recorded parameters included reaction forces, stresses, mid-span deflections, and damage evolution variables, while an integrated output section was used to determine the applied load throughout the simulation. The numerical results were subsequently validated against the experimental load–deflection responses and the observed failure modes, demonstrating good agreement and confirming the reliability and accuracy of the developed finite element model.

5.2. FEA Results and Discussion

5.2.1. Load Deflection Curves

Figure 17 presents a comparison between the average experimental results and the finite element predictions for all tested beams under ambient and elevated temperature conditions, showing the load–deflection curves of each specimen. Overall, the numerical model successfully captured the nonlinear response, stiffness degradation, and post-peak behavior of the reinforced concrete beams incorporating varying RCFA replacement ratios. A clear reduction in load capacity and stiffness with increasing temperature is consistently reflected in both the experimental and FEA curves, confirming the significant influence of thermal exposure on shear performance. In particular, the beams exposed to 600 °C exhibited more pronounced softening behavior and reduced peak response compared to those tested at 23 °C and 400 °C, indicating substantial thermal damage to the concrete matrix and steel reinforcement. Also, Table 10 summarizes the ultimate numerical load, peak numerical deflection, and their percentage differences compared with the experimental results. The numerical predictions show very good agreement with the experimental data. The difference in ultimate load capacity ranges between approximately 1.4% and 5.4% across all specimens, while the variation in peak deflection ranges from about 0.0% to 7.5%. Such deviations remain within acceptable limits for nonlinear finite element simulations of reinforced concrete members subjected to combined mechanical and thermal effects. Minor discrepancies can be attributed to idealizations adopted when modeling the material, particularly in representing crack propagation and bond behavior, as well as assumptions related to the thermal degradation of mechanical properties. Additionally, slight differences in boundary condition representation and load application methods between the numerical model and experimental setup may have contributed to these variations. Nevertheless, the close correlation observed in Figure 16 and quantified in Table 10 confirms the reliability and robustness of the developed finite element model in predicting the shear behavior of RC beams with recycled aggregates under fire exposure.

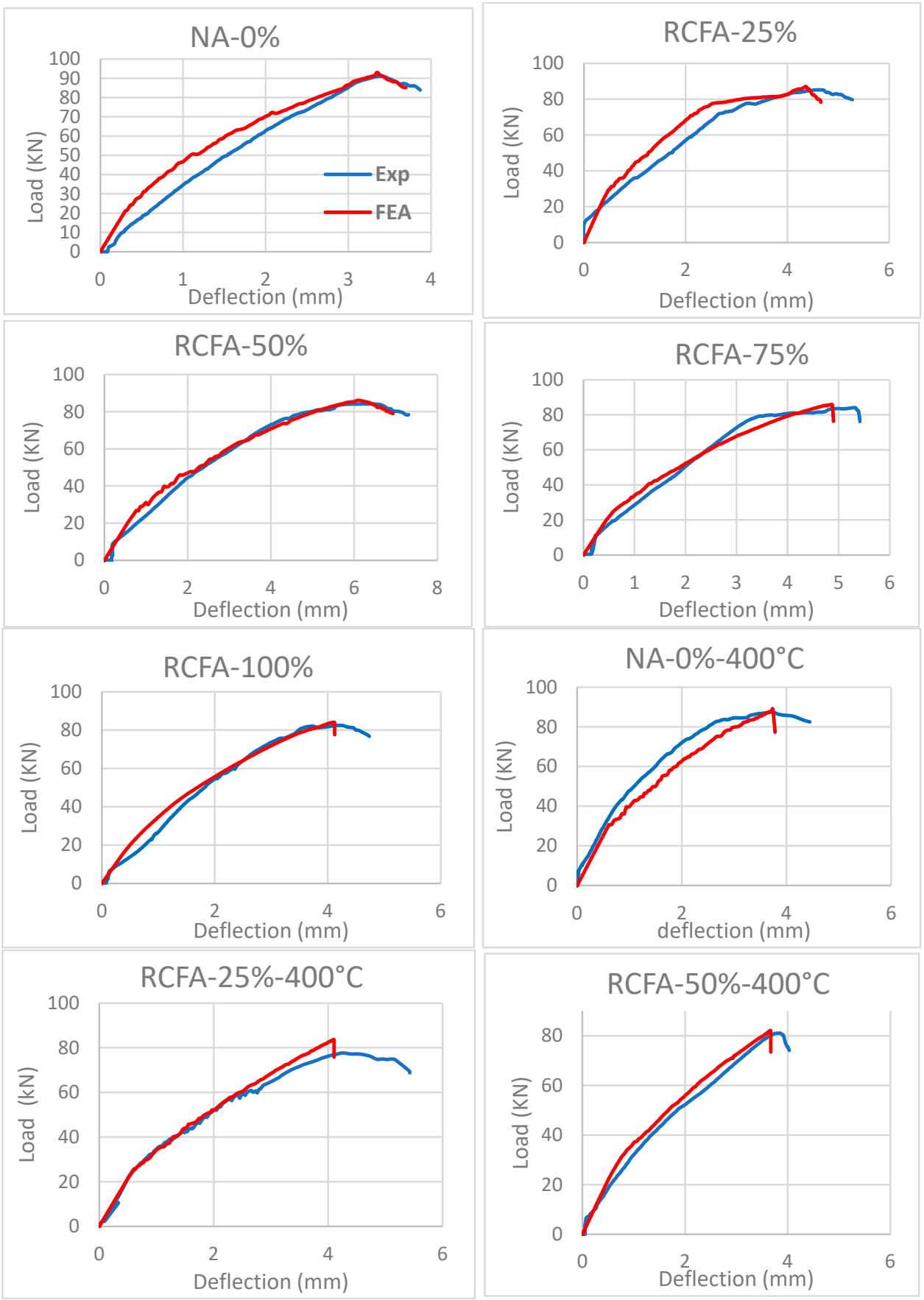


Figure 17. *Cont.*

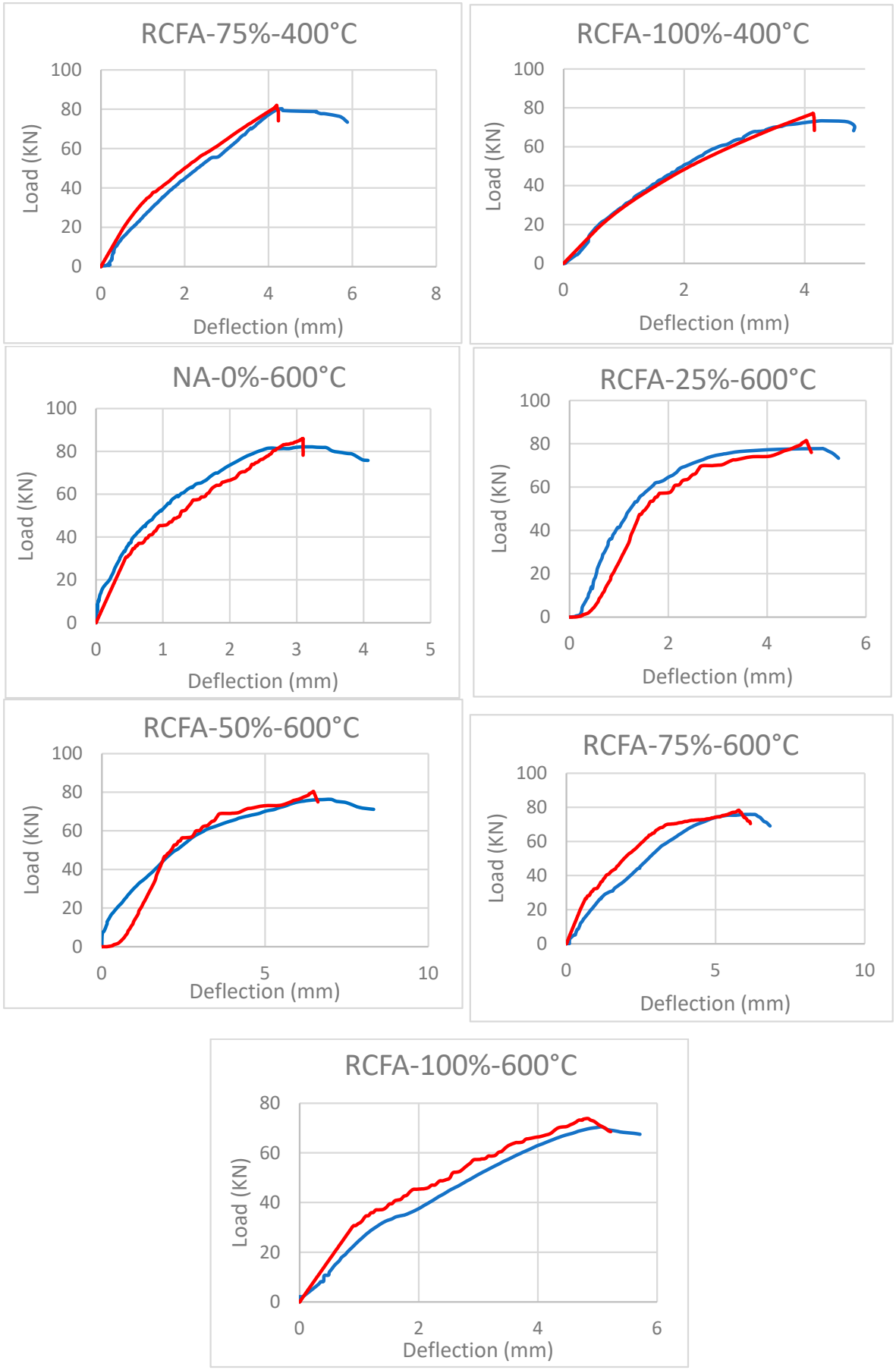


Figure 17. Load-deflection curve for experimental vs. FEA results.

Table 10. Numerical results.

Beam ID	Ultimate Numerical Load (kN)	Ultimate Numerical Load Compared to Experimental Results	Peak Numerical Deflection (mm)	Peak Numerical Deflection Compared to Experimental Results
NA-0%	93.1	2.3%	3.3	−2.9%
RCFA-25%	86.9	2.0%	4.4	−4.3%
RCFA-50%	86.1	2.1%	6.1	−4.7%
RCFA-75%	85.9	2.1%	4.9	−7.5%
RCFA-100%	84	1.9%	4.1	−2.4%
NA-0%-400 °C	89.2	2.1%	3.7	0.0%
RCFA-25%-400 °C	83.7	2.7%	4.1	−4.7%
RCFA-50%-400 °C	82.2	1.4%	3.7	−5.1%
RCFA-75%-400 °C	82	2.1%	4.2	−2.3%
RCFA-100%-400 °C	77.2	4.7%	4.1	−2.4%
NA-0%-600 °C	86	4.8%	3.1	−3.1%
RCFA-25%-600 °C	81.5	4.8%	4.8	−5.9%
RCFA-50%-600 °C	80.4	5.4%	6.5	−7.1%
RCFA-75%-600 °C	78.2	3.0%	5.8	−3.3%
RCFA-100%-600 °C	73.8	4.7%	4.8	−5.9%

5.2.2. Failure Mode

The comparison between the experimental and numerical failure patterns of all tested beams is presented in Figure 18. Strong agreement can be observed between the experimental crack patterns and the damage contours predicted by the finite element model for all RCFA replacement ratios and temperature levels. At ambient temperature, the control beam NA-0% exhibited typical diagonal shear cracking initiated in the shear span and propagating toward the loading point, accompanied by flexural cracks at mid-span. This behavior was accurately reproduced by the numerical model, which showed concentrated damage zones along the main diagonal shear path. Similar crack propagation trends were observed for RCFA-25%, RCFA-50%, RCFA-75%, and RCFA-100%, where diagonal cracking governed the failure mode, confirming that increasing the RCFA content did not alter the fundamental shear failure mechanism.

After exposure to 400 °C, the beams showed more distributed cracking and reduced crack sharpness, indicating stiffness degradation due to thermal damage. The numerical damage patterns reflected the same diagonal shear mechanism with slightly wider damaged zones, consistent with experimental observations. At 600 °C, the failure patterns became more pronounced, with extended diagonal cracks and localized crushing near the compression zone and supports. The finite element results captured these characteristics through intensified damage localization and stress concentration in the same regions.

Overall, Figure 18 demonstrates that the developed nonlinear finite element model successfully predicted the crack initiation, propagation paths, and dominant shear failure modes under both ambient and elevated temperature conditions. Minor differences in crack dispersion may be attributed to modeling idealizations and mesh discretization; however, the general agreement confirms the reliability of the numerical model in simulating shear failure behavior of reinforced concrete beams incorporating recycled aggregates under fire exposure.

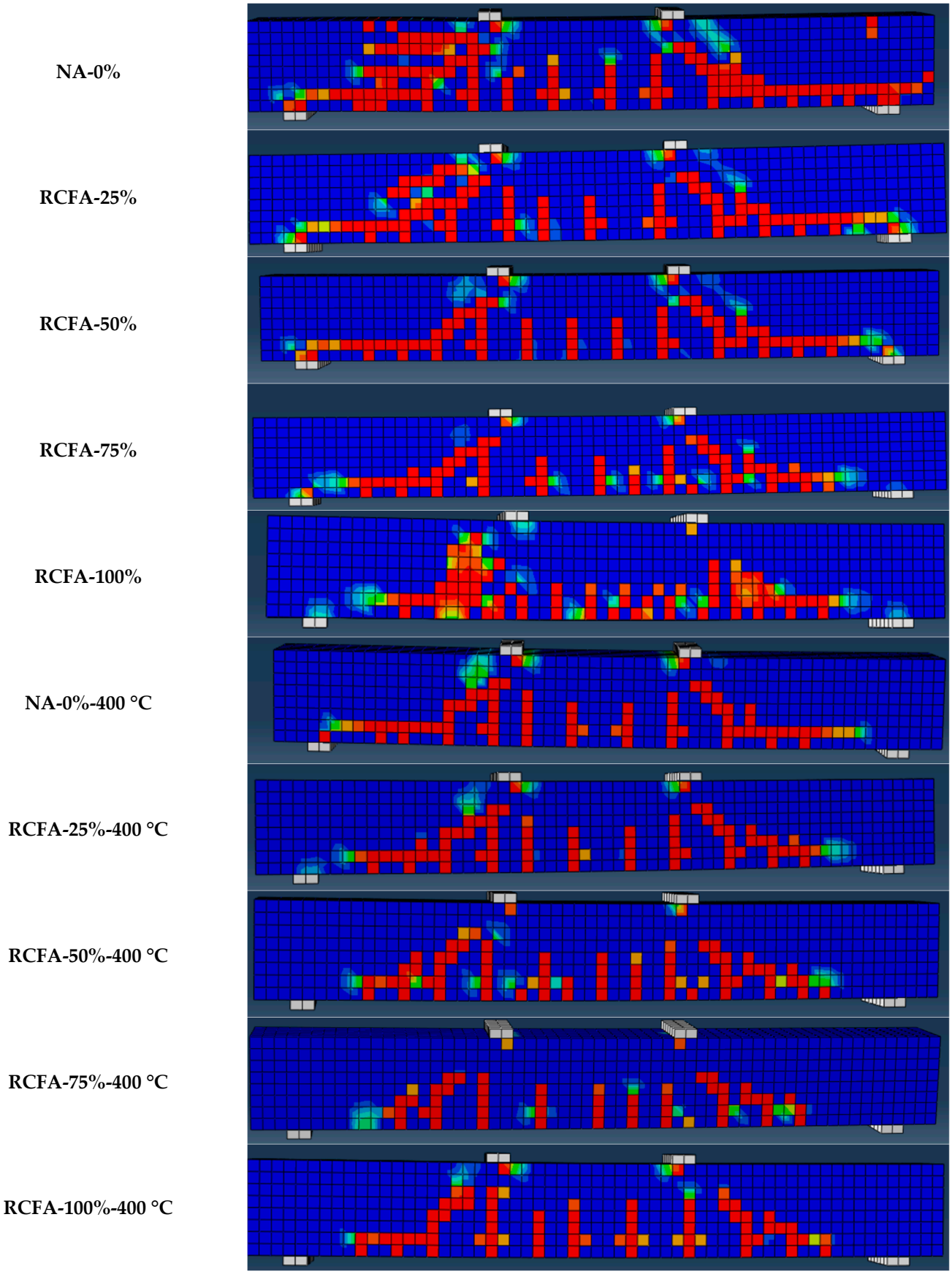


Figure 18. *Cont.*

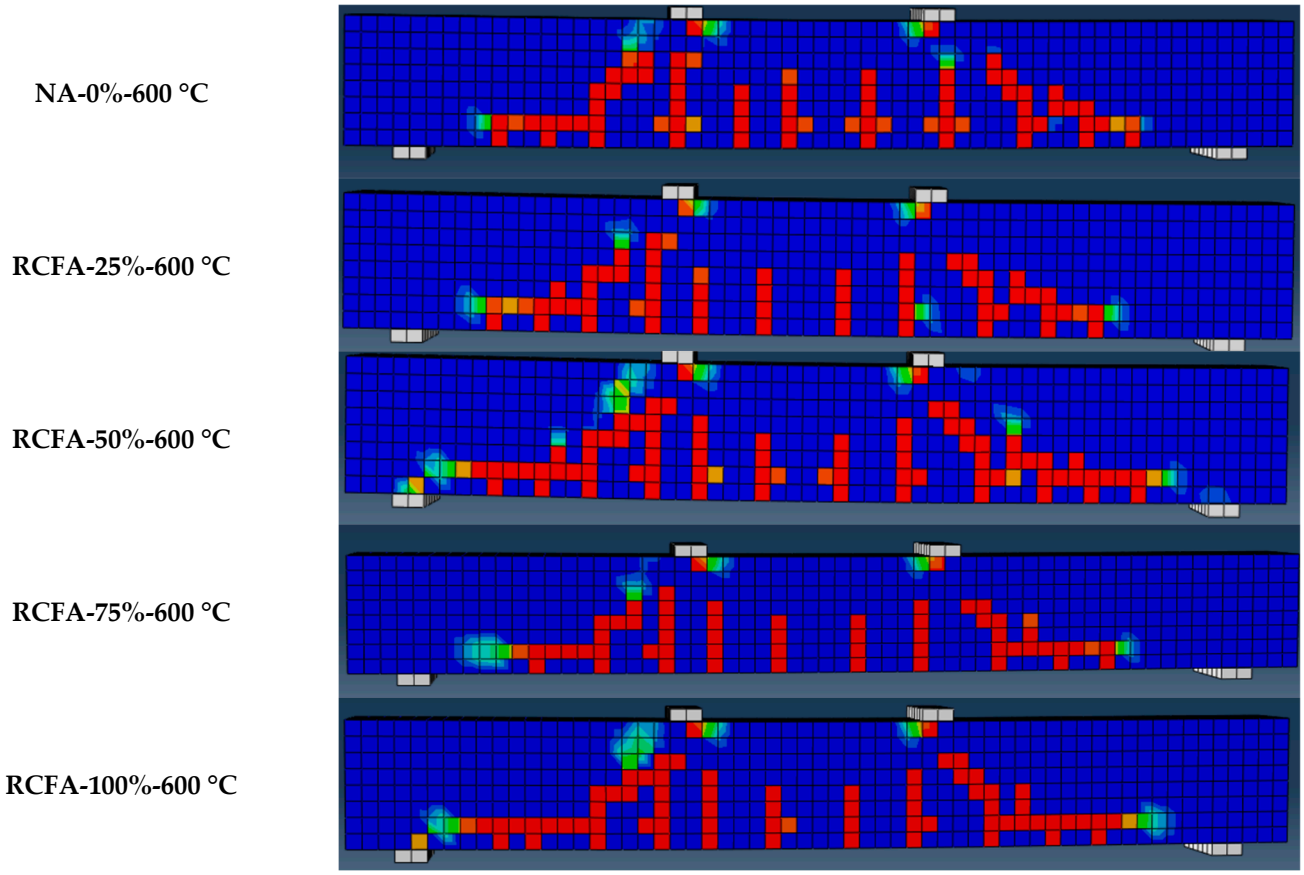


Figure 18. Failure mode for beams by FEA.

6. Conclusions

This study experimentally and numerically investigated the shear performance of reinforced concrete (RC) beams incorporating recycled coarse and fine aggregates (RCFAs) under ambient and elevated temperature conditions (400 °C and 600 °C). The influence of replacement ratio and fire exposure on compressive strength, load–deflection behavior, ultimate load capacity, stiffness, ductility, and failure mode was examined. A nonlinear finite element model was also developed and validated against experimental results. The following conclusions can be drawn:

- Increasing the RCFA replacement ratio led to a gradual reduction in compressive strength at room temperature. After exposure to 400 °C, strength reductions ranged approximately from 2.6% to 9.4%, while at 600 °C, the reductions became more significant, reaching up to about 22%. Mixes with higher replacement levels exhibited greater susceptibility to thermal degradation due to higher porosity and weaker interfacial transition zones.
- The load–deflection response showed clear stiffness degradation with increasing temperature and RCFA content. Beams tested at room temperature exhibited the highest stiffness and load capacity, while those exposed to 600 °C showed pronounced softening behavior and higher peak deflections.
- At ambient temperature, ultimate load decreased moderately with an increasing RCFA content, with reductions ranging between approximately 6% and 10% compared to the control beam. After exposure to 400 °C, additional reductions of about 4–11% were observed, whereas at 600 °C the total reduction reached up to approximately 22% relative to the control beam at room temperature.

- Temperature was found to be the dominant factor affecting shear capacity. While moderate RCFA replacement levels (up to 50–75%) preserved acceptable residual load capacity, full replacement (100%) resulted in a more pronounced reduction, particularly after exposure to 600 °C.
- All beams failed in a classical diagonal shear mode. Although RCFA content and temperature influenced crack initiation load, crack width, and crack density, the fundamental shear failure mechanism remained unchanged. Elevated temperature primarily intensified crack propagation and damage severity rather than altering the failure pattern.
- Moderate RCFA replacement levels improved ductility and energy absorption capacity, particularly under elevated temperature conditions. Beams with partial replacement exhibited more distributed cracking and a more gradual shear failure compared to the relatively more brittle response of the control beam after severe heating.
- The developed finite element model showed very good agreement with the experimental results. Differences in ultimate load ranged between approximately 1% and 5%, while peak deflection variations remained within acceptable limits, confirming the reliability of the numerical simulation in predicting shear behavior under combined mechanical and thermal effects.

Overall, the findings demonstrate that reinforced concrete beams incorporating moderate levels of recycled coarse and fine aggregates can maintain acceptable shear performance under fire exposure. Although elevated temperature significantly reduces load capacity and stiffness, partial replacement levels provide a sustainable alternative without fundamentally compromising structural safety.

7. Recommendations and Future Work

Based on the experimental and numerical findings of this study, it is evident that incorporating recycled coarse and fine aggregates (RCFAs) in reinforced concrete beams subjected to elevated temperatures is feasible at moderate replacement levels; however, higher replacement ratios combined with severe fire exposure significantly affect shear capacity, stiffness, and ductility. Therefore, several research gaps remain that warrant further investigation to ensure safe structural implementation.

- The influence of different heating durations, cooling regimes (air cooling vs. water cooling), and realistic fire curves should be investigated to better simulate actual fire conditions.
- Long-term durability after fire exposure, including residual bond strength, cracking stability, and stiffness recovery, should be systematically evaluated.
- Detailed microstructural analyses (e.g., SEM, XRD, and porosity measurements) are recommended to clarify the thermal degradation mechanisms of the interfacial transition zone in RCFA concrete.
- The effectiveness of strengthening techniques (e.g., steel fibers, FRP systems, or hybrid reinforcement strategies) in enhancing the post-fire shear performance of RCFA beams should be explored.
- Parametric numerical studies using advanced finite element modeling are needed to develop predictive models and propose modification factors for shear design provisions under fire exposure.
- Structure-scale testing of continuous beams, slabs, and frame elements incorporating RCFAs under combined mechanical and thermal loading is necessary to validate practical structural behavior.

- Finally, life-cycle assessment studies integrating structural performance and fire resilience should be conducted to quantify the sustainability benefits of RCFAs in fire-prone structural applications.

Author Contributions: Conceptualization, M.A.-J. and A.A.; methodology, M.S.; software, M.S.; validation, M.S. and A.A.-K.; formal analysis, M.S.; investigation, A.A.-K.; resources, M.S.; data curation, O.S.; writing—original draft preparation, M.S. and O.S.; writing—review and editing, A.A.; visualization, A.A.; supervision, M.A.-J.; project administration, M.S.; funding acquisition, M.A.-J. All authors have read and agreed to the published version of the manuscript.

Funding: This research was funded by the Abdul Hameed Shoman Foundation Scientific Research Fund, grant number 240800482. The APC was funded by the Abdul Hameed Shoman Foundation Scientific Research Fund.

Data Availability Statement: The original contributions presented in this study are included in the article. Further inquiries can be directed to the corresponding author.

Acknowledgments: The authors gratefully acknowledge the support of the Abdul Hameed Shoman Foundation Scientific Research Fund under grant number 240800482.

Conflicts of Interest: The authors declare no conflicts of interest.

Abbreviations

ASTM	American Society for Testing and Materials
NA	Natural Aggregate
NCA	Natural Coarse Aggregate
NFA	Natural Fine Aggregate
RA	Recycled Aggregate
RC	Reinforced Concrete
RCA	Recycled Coarse Aggregate
RCFA	Recycled Coarse and Fine Aggregate
RFA	Recycled Fine Aggregate
RRAC	Reinforced Recycled Aggregate Concrete

References

1. Liu, K.; Fu, K.; Sang, Y.; Yang, Y.; Zou, C.; Xie, T.; Zhao, X. Frost resistance of recycled aggregate concrete: A critical review. *J. Build. Eng.* **2024**, *90*, 109450. [CrossRef]
2. Nguyen, T.-D.; Cherif, R.; Mahieux, P.-Y.; Turcry, P.; Bastidas-Arteaga, E. A review on deterioration Mechanisms, durability prediction and enhancement techniques for recycled aggregate concrete. *Clean. Mater.* **2025**, *16*, 100306. [CrossRef]
3. Alibeigibeni, A.; Stochino, F.; Zucca, M.; Gayarre, F.L. Enhancing Concrete Sustainability: A Critical Review of the Performance of Recycled Concrete Aggregates (RCAs) in Structural Concrete. *Buildings* **2025**, *15*, 1361. [CrossRef]
4. Garg, N.; Shrivastava, S. A review on utilization of recycled concrete aggregates (RCA) and ceramic fines in mortar application. *Mater. Today Proc.* **2023**, *73*, 64–73. [CrossRef]
5. Tam, V.W.; Soomro, M.; Evangelista, A.C.J. Quality improvement of recycled concrete aggregate by removal of residual mortar: A comprehensive review of approaches adopted. *Constr. Build. Mater.* **2021**, *288*, 123066. [CrossRef]
6. Joseph, H.S.; Pachiappan, T.; Avudaiappan, S.; Maureira-Carsalade, N.; Roco-Videla, Á.; Guindos, P.; Parra, P.F. A Comprehensive Review on Recycling of Construction Demolition Waste in Concrete. *Sustainability* **2023**, *15*, 4932. [CrossRef]
7. Recycled Concrete Aggregates Market Poised for Sustainable Growth and Innovation. Precedence Research. 2025. Available online: https://www.precedenceresearch.com/recycled-concrete-aggregates-market?utm_source.com (accessed on 23 January 2026).
8. Silva, R.V.; De Brito, J.; Dhir, R.K. Properties and composition of recycled aggregates from construction and demolition waste suitable for concrete production. *Constr. Build. Mater.* **2014**, *65*, 201–217. [CrossRef]
9. Bu, C.; Liu, L.; Lu, X.; Zhu, D.; Sun, Y.; Yu, L.; OuYang, Y.; Cao, X.; Wei, Q. The Durability of Recycled Fine Aggregate Concrete: A Review. *Materials* **2022**, *15*, 1110. [CrossRef]
10. Berredjem, L.; Arabi, N.; Molez, L. Mechanical and durability properties of concrete based on recycled coarse and fine aggregates produced from demolished concrete. *Constr. Build. Mater.* **2020**, *246*, 118421. [CrossRef]

11. Liang, C.; Bao, J.; Gu, F.; Lu, J.; Ma, Z.; Hou, S.; Duan, Z. Determining the importance of recycled aggregate characteristics affecting the elastic modulus of concrete by modeled recycled aggregate concrete: Experiment and numerical simulation. *Cem. Concr. Compos.* **2025**, *162*, 106118. [CrossRef]
12. Akbulut, Z.F.; Guler, S.; Yavuz, D.; Avcı, M.S. Toward sustainable construction: A critical review of recycled aggregate concrete properties and future opportunities. *Case Stud. Constr. Mater.* **2025**, *23*, e05133. [CrossRef]
13. Etman, E.E.; Hussein, M.; Kassem, N.M.; Nabil, A.; Abdel-Aziz, M.A. Investigation of shear behavior of RC beams incorporating recycled coarse aggregate. *Structures* **2025**, *78*, 109282. [CrossRef]
14. Al Mahmoud, F.; Boissiere, R.; Mercier, C.; Khelil, A. Shear behavior of reinforced concrete beams made from recycled coarse and fine aggregates. *Structures* **2020**, *25*, 660–669. [CrossRef]
15. Wardeh, G.; Ghorbel, E. Shear strength of reinforced concrete beams with recycled aggregates. *Adv. Struct. Eng.* **2019**, *22*, 1938–1951. [CrossRef]
16. Mathew, M.; Girija, K.; Sreedevi, A.R. Shear behaviour of reinforced concrete beams using treated recycled coarse aggregates and steel fibres. *Mater. Today Proc.* **2024**. [CrossRef]
17. Gao, D.; Zhu, W.; Fang, D.; Tang, J.; Zhu, H. Shear behavior analysis and capacity prediction for the steel fiber reinforced concrete beam with recycled fine aggregate and recycled coarse aggregate. *Structures* **2022**, *37*, 44–55. [CrossRef]
18. Hossain, F.Z.; Pal, A.; Ahmed, K.S.; Bediwy, A.; Alam, M.S. Shear behavior of polypropylene fiber-reinforced concrete beams containing recycled aggregate and crumb rubber. *J. Clean. Prod.* **2023**, *412*, 137370. [CrossRef]
19. Saberian, M.; Shi, L.; Sidiq, A.; Li, J.; Setunge, S.; Li, C.-Q. Recycled concrete aggregate mixed with crumb rubber under elevated temperature. *Constr. Build. Mater.* **2019**, *222*, 119–129. [CrossRef]
20. Shhabat, M.; Ashteyat, A.; Abdel-Jaber, M. Repairing of One-Way Solid Slab Exposed to Thermal Shock Using CFRP: Experimental and Analytical Study. *Fibers* **2024**, *12*, 18. [CrossRef]
21. Hisbani, N.; Shams, M.A.; Stanikzai, M.A.; Almujibah, H.; Benjeddou, O. Flexural performance of reinforced concrete beams exposed to uncontrolled fire with and without plaster protection. *Sci. Rep.* **2025**, *15*, 31361. [CrossRef]
22. Ashteyat, A.; Shhabat, M.; Al-Hazmi, I. Repairing high-strength concrete two-way solid slabs exposed to elevated temperature using NSM-CFRP ropes. *Compos. Part C Open Access* **2025**, *17*, 100590. [CrossRef]
23. Azevedo, A.; Firmo, J.; Correia, J. Fire behaviour of reinforced concrete beams strengthened in shear according to the embedded through-section (ETS) technique: Experimental and numerical study. *Compos. Struct.* **2025**, *357*, 118888. [CrossRef]
24. Ashteyat, A.; Shhabat, M.; Al-Khreisat, A.; Aldawsari, S. Shear Behavior of Reinforced Concrete Two-Way Slabs with Openings. *Buildings* **2025**, *15*, 2765. [CrossRef]
25. Ashteyat, A.; Shhabat, M.; Aljarah, A.H.; Al-Zu'bI, H.; Alkhalaileh, A.; Al-Khreisat, A.; Abdel-Jaber, M. Shear strengthening of two-way reinforced concrete slabs with openings: A review of strengthening techniques and code perspectives. *Results Eng.* **2025**, *28*, 108059. [CrossRef]
26. Abdel-Jaber, M.; Magharbeh, L.; Shhabat, M.; Ashteyat, A. Strengthening and repairing of a one-way solid slab exposed to thermal effect using CFRP Grid. *Compos. Part C Open Access* **2026**, *19*, 100694. [CrossRef]
27. Lin, L.; Xu, J.; Ying, W.; Yu, Y.; Zhou, L. Post-fire compressive mechanical behaviors of concrete incorporating coarse and fine recycled aggregates. *Constr. Build. Mater.* **2025**, *461*, 139948. [CrossRef]
28. Zhang, X.; Zhu, Y.; Shen, Y.; Wang, J.; Fan, Y.; Gao, X.; Huang, Y. Compressive mechanical performance and microscopic mechanism of basalt fiber-reinforced recycled aggregate concrete after elevated temperature exposure. *J. Build. Eng.* **2024**, *96*, 110647. [CrossRef]
29. Amin, M.; Hakeem, I.Y.; Zeyad, A.M.; Tayeh, B.A.; Maglad, A.M.; Agwa, I.S. Influence of recycled aggregates and carbon nanofibres on properties of ultra-high-performance concrete under elevated temperatures. *Case Stud. Constr. Mater.* **2022**, *16*, e01063. [CrossRef]
30. Abedalqader, A.; Shatarat, N.; Ashteyat, A.; Katkhuda, H. Influence of temperature on mechanical properties of recycled asphalt pavement aggregate and recycled coarse aggregate concrete. *Constr. Build. Mater.* **2021**, *269*, 121285. [CrossRef]
31. Zheng, W.; Pan, Z.; Chen, Z.; Xu, J.; Xiao, J.; Chen, W. Shear behavior of reinforced recycled aggregate concrete beams after exposure to temperatures up to 600 °C. *Eng. Struct.* **2021**, *244*, 112756. [CrossRef]
32. Song, Y.; Fu, C.; Liang, S. Residual Shear Capacity of RC Beams Without Stirrups After Fire Exposure. *Buildings* **2022**, *12*, 1706. [CrossRef]
33. Yu, Y.; Zheng, Y.; Guo, Y.; Hu, S.; Hua, K. Mesoscale finite element modeling of recycled aggregate concrete under axial tension. *Constr. Build. Mater.* **2021**, *266*, 121002. [CrossRef]
34. *EN 1994-1-2 (2005)*; Eurocode 4: Design of Composite Steel and Concrete Structures—Part 1–2: General Rules—Structural Fire Design. ECS, European Committee for Standardization: Brussels, Belgium, 2011; Volume 1. (In English)
35. *ACI 318M-19*; Building Code Requirements for Structural Concrete. American Concrete Institute: Farmington Hills, MI, USA, 1989; Volume 2007.

36. *ASTM C192/C192M*; Standard Practice for Making and Curing Concrete Test Specimens in the Laboratory. ASTM International: West Conshohocken, PA, USA, 2023.
37. Vieira, J.; Correia, J.; de Brito, J. Post-fire residual mechanical properties of concrete made with recycled concrete coarse aggregates. *Cem. Concr. Res.* **2011**, *41*, 533–541. [CrossRef]
38. Chen, G.; He, Y.; Yang, H.; Chen, J.; Guo, Y. Compressive behavior of steel fiber reinforced recycled aggregate concrete after exposure to elevated temperatures. *Constr. Build. Mater.* **2014**, *71*, 1–15. [CrossRef]
39. Guo, Z.; Chen, C.; Lehman, D.E.; Xiao, W.; Zheng, S.; Fan, B. Mechanical and durability behaviours of concrete made with recycled coarse and fine aggregates. *Eur. J. Environ. Civ. Eng.* **2020**, *24*, 171–189. [CrossRef]
40. Chen, Z.; Xu, R.; Liang, H. Residual mechanical properties and numerical analysis of recycled pebble aggregate concrete after high temperature exposure and cooled by fire hydrant. *Constr. Build. Mater.* **2022**, *319*, 126137. [CrossRef]
41. Choi, H.; Ju, M.; Razakamandimby, R.D.F.T.; Park, K. Cohesive zone modeling of crack propagation, branching, and coalescence in multiphase composites. *Comput. Mech.* **2025**, *76*, 227–250. [CrossRef]
42. De Maio, U.; Gaetano, D.; Greco, F.; Lonetti, P.; Pranno, A. An adaptive cohesive interface model for fracture propagation analysis in heterogeneous media. *Eng. Fract. Mech.* **2025**, *325*, 111330. [CrossRef]
43. Yeon, Y.-M.; Lee, W.; Hong, K.-N. Finite element analysis of reinforced concrete beams prestressed by Fe-based shape memory alloy bars. *Appl. Sci.* **2022**, *12*, 3255. [CrossRef]
44. Usidamen, D.; Ogirigbo, O.R.; Nwankwo, E. An experimental and numerical evaluation of the structural performance of bamboo-reinforced concrete beams. *Discov. Civ. Eng.* **2024**, *1*, 147. [CrossRef]

Disclaimer/Publisher's Note: The statements, opinions and data contained in all publications are solely those of the individual author(s) and contributor(s) and not of MDPI and/or the editor(s). MDPI and/or the editor(s) disclaim responsibility for any injury to people or property resulting from any ideas, methods, instructions or products referred to in the content.